

Research



Article submitted to journal

Subject Areas:

planetary astrophysics, orbits, minor planets.

Keywords:

stellar occultations, satellites, Weywot, Vanth, orbits, TNBs, small solar system objects, formation.

Author for correspondence:

Felipe Braga Ribas

e-mail: fribas@utfpr.edu.br

Investigating the formation of small Solar System objects using stellar occultations by satellites: present, future and its use to update satellite orbits

F. Braga-Ribas^{1,2,3}, F. Vachier⁴,J. Desmars^{4,5}, G. Margoti^{1,2,3}, B. Sicardy⁴

¹Federal University of Technology - Paraná (PPGFA/UTFPR), Curitiba, PR, Brazil; ²Laboratório Interinstitucional de e-Astronomia - LIneA, Rio de Janeiro, RJ, Brazil; ³Observatório Nacional/MCTI, Rio de Janeiro, RJ, Brazil; ⁴Institut de Mécanique Céleste et de Calcul des Éphémérides, IMCCE, Observatoire de Paris, PSL Research University, CNRS, Sorbonne Universités, UPMC Univ Paris 06, Univ. Lille, France; ⁵Institut Polytechnique des Sciences Avancées IPSA, 94200 Ivry-sur-Seine, France;

The history of the outer solar system is intrinsically related to the Giant Planets migration. A massive disk of material within a radius of 30 au was scattered during the planetary migration, creating different dynamic populations in the Transneptunian region. They were formed in a collisional environment when massive collisions allowed them to grow and form much smaller moons than the primary body. The dynamical group, known as the Cold Classics, was formed in a sparse disk from 42 to about 47 au and did not suffer much from planet migration. Observations show that many of Cold Classical are binary, consistent with the streaming instability process. The stellar occultation technique, with a spatial resolution of a few kilometres, can be used to search for binaries where other techniques are unable to do so, and to characterise the known satellites of Trans-Neptunian Objects (TNO), constraining their formation scenarios. We review here the first stellar occultations by TNO's satellites (besides Charon), discuss the methods used to detect these events. We also fit new orbital elements and system mass for Vanth (Orcus/1) and Weywot (Quaoar/1), finding reasonable solutions for pure Keplerian orbits. Finally, we discuss the prospects regarding the stellar occultations by TNO binaries and their implications for the study of the history of the Solar System.

1. Introduction

The complete history of the Outer Solar System's current structure is yet under discussion. In short, many works have shown that the Giant Planets were formed in a tighter configuration closer to the Sun. After a few hundred million years, they migrated outwards, scattering a massive disk of planetesimals that existed inside 30 au [1–4]. These objects fed the Kuiper Belt's dynamical regions occupied by the Hot Classical (HC), Resonant populations, such as the Plutinos, and the Scattered Disk Objects (SDO) [5,6]. Another dynamical group, the Cold Classical (CC), had a different history [7,8]. They were formed in a sparse disk from 42 to about 47 au and did not suffer much from planet migration.

Stellar occultation has proven to be a powerful technique for studying the Transneptunian region [9,10]. With a spatial resolution of a few kilometres, independent of the object's distance, which is ultimately limited by the Fresnel diffraction and stellar diameter, it has led to the discovery of rings around small objects, such as the Centaur (10199) Chariklo [11], the dwarf-planet (136108) Haumea [12] and the TNO (50000) Quaoar [13,14]. It has also been used to monitor Pluto's atmosphere [15], study TNO's topography [16,17], and provide precise astrometric positions [18]. As discussed further in this Section, this resolution can be used to study the close environment of small objects of the outer Solar System and their satellites. It also allows us to search for putative companions where other techniques are unable to investigate. This comes in a context where the number of TNO satellites became a fundamental information to constrain the formation scenarios.

The Cold Classicals are small bodies with low orbital inclinations and eccentricity, formed in a low collisional environment. Observations show that more than 30% of Cold Classicals are found to be binaries, with equal size and similar colour of the components [19]. All this is consistent with an in situ formation through the streaming instability process, which predicts that most (if not all) planetesimals are formed in binary or multiple systems [20].

In contrast, the Hot Population objects (HP)¹ were formed and grew in a collisional environment (a massive planetesimal disk) and then transported to their current positions through scattering encounters with Neptune [21]. Differently from the CCs, the majority of the moons of the HP are much smaller than the primary (with a radius ratio < 0.5), and almost all of the most prominent members (with radii $R > 500$ km) have known satellites. This indicates that they were accreted from a disk around the primary, which, in turn, was formed from a collision of two planetesimals [22,23], a condition only found in the massive planetesimal disk, prior to their implementation at their current location. It was shown that 50% of the bound binaries with $a_B/R_B < 30$ (where a_B is the binary semi-major axis and $R_B = (R_1^3 + R_2^3)^{1/3}$, being R_1 and R_2 the radii of each component) survive the implementation to the HP region. The wide binaries instead did not survive, so they may have originated before scattering in a rarefied part of the disk beyond 30 au [20].

Most of this scenario is based on the interpretation of the numerical simulations, which are, in turn, bounded by direct observations of the objects, e.g., their relative sizes, colours, and presence and orbit of satellites. In many cases, sizes are based on assumptions of colours and albedos or via observations on the thermal region of the spectrum, and most of the satellites or binaries were discovered using high-resolution images. These techniques have their caveats and limitations. For instance, observations have shown that at least 30% of the CCs are binaries [24], but this is based mainly on Hubble Space Telescope (HST) observations. HST's best resolution is 40 milli-arcsec (mas) in the plane of the sky, which translates to a spatial resolution of about 1200 km at 42 au. Therefore, binaries or satellites closer to this distance are blended in the images, so they can not be firmly detected with direct images [25].

Considering the context presented above, some unanswered questions that can help narrow the formation scenarios and determine the global properties of TNBs remain to be addressed:

- Are all the Cold Classicals binaries?
- Are small satellites a rare property in the Cold Classicals region?
- Is there a gap between being a (separated) binary system and a contact binary object?
- Are the hot population moons similar to the primary in terms of composition and density?

¹By Hot Population we refer to the Hot Classical, Resonant population, and the Scattered Disk Objects.

- Do the satellites have the same albedo as the primary? Therefore, are albedo-based sizes a good estimation?
- How many satellites were formed after the implantation in the hot population region?
- Do rings exist in the Cold Classicals region, or do they need a collisional active environment to be formed?

The stellar occultation technique can be used to probe the TNO's close environments, study the TNO's satellites, search for unknown companions or reveal binarity. The chances of detecting an unknown component are small; still, detecting one of the components already brings valuable information, such as the position of the secondary relative to the primary. The precision so obtained is comparable to that derived with high-resolution images from ground-based or space telescopes. It can also be related to information from other techniques, such as astrometric wobbling and thermal size determination [10].

Observation of occultations by TNO satellites or binaries (TNOBs, for short) is still rare. A few stellar occultations by Charon, Pluto's main satellite, were used to determine its size and constrain its orbit [26]. The first stellar occultation observed by a TNOB, after Charon, was caused by Vanth, the satellite of (90482) Orcus, on March 1, 2014 [27]. In March 2017, a fortuitous observation of another occultation by Vanth allowed determine its size, assuming spherical, with a diameter of 443 ± 10 km [28]. Two stellar occultations by Hi'iaka, the biggest satellite of (136108) Haumea, were predicted and detected in April 2021, constraining the satellite's size and shape [29] (Fernandez-Vallenzuela, 2024, *submitted*). The Plutino (523764) 2014 WC₅₁₀ was discovered to be a similar-sized binary during a stellar occultation in December 2018 [30]. Observations of occultations by the Hot Population satellites of (50000) Quaoar [31], (38628) Huya [32], (82075) 2000 YW₁₃₄ [33], (19521) Chaos [34], and (120347) Salacia have been reported².

In this section, we have discussed the connection between the Solar System's history and the formation of binaries, and we have provided the current list of stellar occultations by TNO satellites that we are aware of. In Section 2, we will discuss the methods used to detect secondary events, either by chance or predicted from satellite ephemerides. In Section 3, we will present new orbit and mass parameters obtained for the Orcus and Quaoar systems based on positions derived from stellar occultations. The implications of these results will be addressed in Section 4, where we will also consider why the number of recorded stellar occultations by TNOBs (especially for the CCs) will greatly increase in the near future.

2. Observing Stellar Occultations by TNO Satellites

Detecting a stellar occultation by a TNO satellite can result from i) a lucky observation or ii) a predicted event.

(a) Lucky detection

When an occultation event is recorded, a secondary drop in the light curve may be detected. If the secondary event is as deep as the (expected) flux drop caused by the main body, it may be caused by a satellite. In the opposite case, if the drop is not as deep as expected by the primary body, then it may stem from either a semi-transparent ring or from the presence of a companion star. An unexpected secondary drop may be associated with a known satellite if the chord length and relative distance to the primary can be correlated to the known properties of the moon [32].

To increase the chances of secondary detection, observations should last long enough to probe the object's environment. The duration will depend on the expected semi-major axis of the satellite and the event's velocity (typically 20 km s^{-1}). The currently known TNO binary with the largest separation (more than 103500 km) is 2001 QW₃₂₂. This corresponds to almost three hours of observations for the star to cross both sides of the satellite's orbit, however, this is an extreme case. Out of the 145 known semi-major axes of TNOBs³, 65% need only 15 minutes of observation, 73% need up to 30 minutes and 92% less than an hour (Fig. 1).

²From [35], <https://occultations.ct.utfpr.edu.br/results/> updated on September 07, 2024.

³Compilation made by Johnston, Wm. Robert, <https://www.johnstonsarchive.net/astro/asteroidmoonsall.html> updated on May 27, 2024.

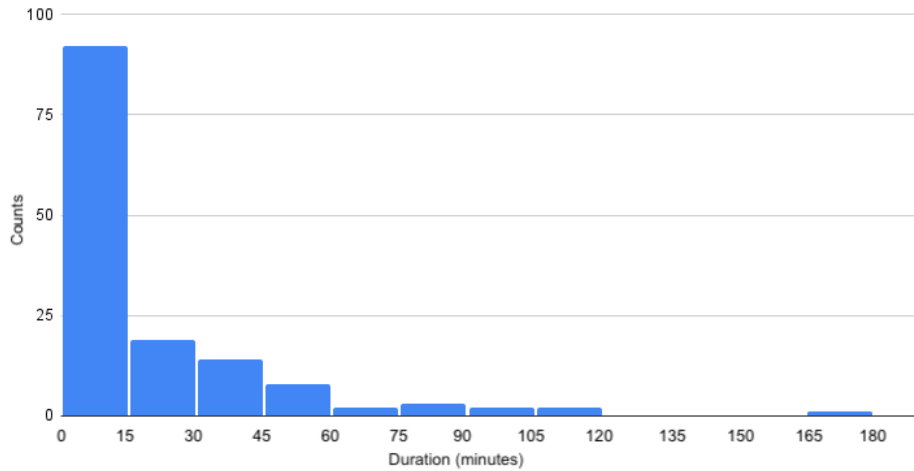


Figure 1. Histogram of the number of known TNOs with known semi-major axis and the total observation interval, in minutes, around the main body event to reach the satellite distance, considering the typical event velocity of 20 km s^{-1} . One-hour long observation can probe 92% of the known TNOs orbits on both sides relative to the central body.

To estimate the largest distance of a putative satellite, we can use the object's half Hill's sphere, which depends on its distance to the Sun (or other nearby objects, such as a Giant Planet [36]) and its mass. Considering their distances from the Sun, using this criterion implies an unrealistic long observation runs of hundreds of hours. Meanwhile, it is expected that a satellite will disintegrate if it gets too close to the main body (roughly 2.5 radii of the main body). This is the Roche limit, which depends on the relative masses and radius of the secondary [37]. But this is just a crude estimation, as the object's cohesion force can be strong enough to avoid its disruption, especially for similar-sized bodies.

Another approach is to place a number of telescopes in a "fence" distribution perpendicular to the shadow motion, which is typically along the East-West direction. The telescopes must be spaced by at maximum half of the object's expected diameter, over a thousand kilometres, centred at the predicted shadow path. This is especially suitable for surveying the Cold Classicals searching for close binary objects [30].

(b) Prediction

To predict a stellar occultation, both i) the position of the target object in time (i.e., its ephemeris) and ii) the position of a star on its path, for a given observer, need to be known with a precision equivalent to the apparent size of the object in the plane of the sky, roughly, tens of mas. The *Gaia* catalogue provides position, for most stars brighter than magnitude 21 [38], with uncertainties that are much smaller than the apparent sizes of the TNOs. The challenge is thus to determine the satellite ephemeris. For that purpose, precise positions relative to the central body are needed. They are usually obtained with space telescopes (like HST) or large ground-based telescopes (like Keck) with high-resolution imaging capacity, i.e., adaptive optics. This means a high pressure put on these instruments, and thus difficulties in obtaining observing time.

In this work, we use the GENOID algorithm (GENetic Orbit IDentification) [39,40] to fit an orbital model on the known satellite observations in the study. It is a genetics-based algorithm to find the most appropriate set of dynamic parameters, i.e., minimum χ^2 . We start modelling the satellite's motion around the main body with a Keplerian model [41]; if the residuals are significant with respect to the quality of the data (i. e. tens of mas), non-Keplerian perturbations such as the dynamical oblateness J_2 of the primary and the satellite masses can be considered.

GENOID can give precise ephemeris of the satellite relative to the main body, depending on the number and quality of the available positions, through the Miriade ephemeride hosted by

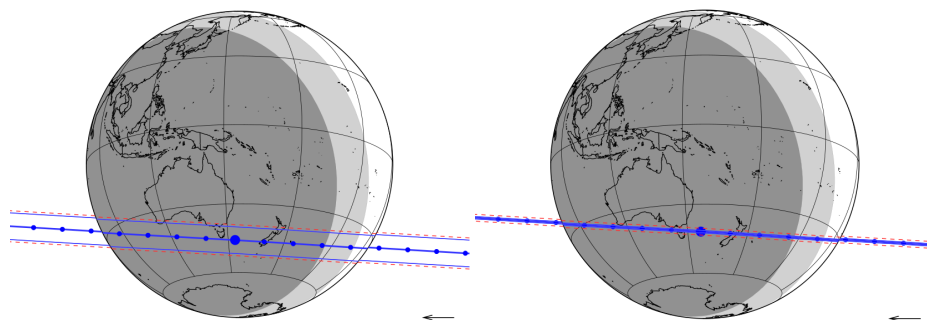


Figure 2. Prediction of an occultation by Quaoar (left) and its satellite Weywot (right) on May 26, 2023. The parallel blue lines, separated by the object's expected diameter, are the shadow paths on Earth. The arrow indicates the direction of the shadow motion, the dots are separated by one minute. The 1σ expected uncertainty is shown as red dashed lines and are plotted relative to the shadow limits (not its centre).

the IMCCE laboratory at Paris Observatory⁴. Like all orbit-fitting algorithms, GENOID requires at least three sufficiently precise primary-to-satellite relative positions, well-distributed in time and space, to obtain an acceptable solution for orbital parameters along with their uncertainties. It is able to deliver robust results when dealing with small and poorly distributed datasets, investigating all the space of parameters. However, if the dataset is sufficient, it offers little advantage compared to less computationally demanding methods (e.g., variational methods [42]).

For the on-sky position calculation, we used the NIMA ephemeris [43], which is designed to provide precise ephemeris for a short period, using Minor Planet Center and proprietary data, as well as occultation-based astrometry when available. The relative offset of the satellite, calculated with GENOID, is applied to the main body's ephemeris, calculated with NINA, to obtain the satellite's position and then compare it to the *Gaia* star catalogue. The predictions are available on the Lucky Star webpage⁵. This method was used to successfully predict the two occultations observed by Hi'iaka in April 2021^{6,7} and occultations by Vanth and Weywot, which will be detailed in this work. Figure 2 gives an example of a predicted occultation involving Quaoar and its satellite Weywot, which eventually yielded the detection of both objects on May 26, 2023.

3. Orbits

As previously mentioned, the satellites Vanth (Orcus/1) and Weywot (Quaoar/1) have already been detected during stellar occultations. Here, we use the relative positions derived from these detections to derive new orbits. The relative position can be accurate to the sub-mas level when multiple chords are detected for both the main body and the satellite, that is, when both objects are detected from several sites during the same event. The on-sky positions of their respective centres can then be pinned down with an accuracy of a few kilometres.

If they are detected from only one site, then two solutions are possible, one with the centre to the North of the chord and one with the centre to the South of the chord [18]. In this case, due to the unknown size of the satellite, the centre uncertainty may be bounded by the expected object's radius (assumed to be spherical), corresponding to a few mas at the TNOs distances. However, both Vanth and Weywot may be non-spherical, which can produce an elongated limb of apparent semi-axes a' and b' and introduces an additional cause of error. We will have a smaller error in the direction of the apparent motion (along-track) and a larger error in the perpendicular

⁴<https://ssp.imcce.fr/forms/ephemeris>

⁵<https://lesia.obspm.fr/lucky-star/>

⁶http://fredvachier.free.fr/binaries/occult/2021/2021-04-06T23_33_52_136108_NIMAv72020Oct21_Binary_solution_1_Kepler/

⁷http://fredvachier.free.fr/binaries/occult/2021/2021-04-16T06_29_54_136108_NIMAv72020Oct21_Binary_solution_1_Kepler/

direction of motion (across-track), see [44]. In an extreme case, where the limb apparent oblateness is $\epsilon' = (a' - b'/a') = 0.5$, this will induce an error of about half of a' , i.e. an additional error of at most $R_{\text{equiv}}/(2\sqrt{1-\epsilon}) = R_{\text{equiv}}/\sqrt{2}$ for $\epsilon < 0.5$.

When only the satellite is detected occulting the star, the relative position is obtained from the ephemeris of the main body. (i) If the main body ephemeris uses positions derived from occultations [45], the relative positions may be obtained, depending on the number of positions and their time-span, with uncertainties in the order of the mas, i.e. a few tens of kilometres. (ii) On the other hand, if only classical astrometry of the system is available, then the primary body position can have an uncertainty of tens of mas, i.e. hundreds of kilometres. In this case, the position of the main body also needs to be corrected from the photo-centric offset caused by the satellite contribution to the total flux [46], as the ephemeris provides not the position of the central body but for the system photocenter. Therefore, the relative uncertainty may be poorly constrained.

Using any relative position is important as they can constrain the orbital solution when only a few relative points are available, which is usually the case. Thus, the mere fact that the satellite occulted the star at a given time already provides the satellite position with an uncertainty comparable to its diameter, corresponding to a few mas on the sky, as mentioned earlier. This is comparable to the accuracy obtained with space- or ground-based telescopes, which is thus useful in improving the satellite's orbital solution. Further analysis of the detected event can reduce the uncertainty; nevertheless, this extra precision will have little impact on the quality of the orbit fit, considering that it also uses relative positions derived from direct imaging with their own uncertainties.

In this work, we use satellite offset positions (X, Y) ⁸ relative to the primary calculated from the reported occultations, limiting our precisions to the satellite's radius (assuming a spherical body, as discussed earlier), together with published offsets⁹, to fit the dynamical parameters of the system: mass (M), orbital period (P), semi-major axis (a), eccentricity (e), inclination (i), longitude of the node (Ω), argument of pericentre (ω), and time of passage at pericentre (t_p). If needed, the algorithm also fits the satellite masses and the J_2 factor related to the object's oblate gravity field [47]. After setting a grid of test values, they are refined, generation after generation, until no significant improvement is obtained, i.e., the residuals of the data points compared to the fitted orbit cease to reduce.

(a) Vanth (Orcus/1)

Orcus is one of the largest Plutino objects, which is an object locked in the 2:3 mean motion resonance with Neptune. It has an estimated diameter of 910 ± 50 km and a high albedo of 0.23 ± 0.02 [48]. Its only known satellite, Vanth, is about 2.4 magnitudes fainter, with an albedo-dependent diameter from 280 to 380 km [49]. Previous works [24,49,50] reported an almost circular orbit, with a period of 9.5 days and a semi-major axis of about 9000 km.

Two stellar occultations by Vanth have been detected so far. The first one was also the first stellar occultation by a TNO satellite ever observed, apart from the Pluto-Charon system [26], and was detected in March 2014. The second detection occurred in March 2017, when two chords allowed an estimate of its diameter, assuming a circular limb to be 443 ± 10 km [28].

(i) March 01, 2014

The first stellar occultation by Vanth was detected on March 1st, 2014, at the Nayoro Observatory, Hokkaido, Japan [27]. Predictions made with the methods described in [51] identified an occultation of the TYC 5476-00882-1 star ($V_{\text{mag}} = 12.1$) by Orcus crossing the South of Australia and New Zealand. Using GENOID-based ephemeris for Vanth, we found that the satellite could cross Japan. An extensive campaign was set to detect both objects, but eventually, only the satellite was detected.

From the observation, a 73.7 ± 3.2 km chord was obtained. Therefore, two on-sky positions for Vanth's centre are equally possible, one considering the centre to the North of the observed chord and the other where the centre is to the South of it. The astrometric position is derived by

⁸The offset (X, Y) gives the apparent differential coordinates of the satellite relative to the primary, as seen in the sky plane.

⁹Here we used the offset values available in Grundy's web page (<https://www2.lowell.edu/users/grundy/tnbs/>), which were reanalysed with their tools to provide a consistent data set, as explained in [24].

fitting the 443 km diameter from [28] and considers the propagated Gaia DR3 position. Using the latest NIMAv10 ephemeris for Orcus, with an estimated uncertainty of 4 mas, we can calculate the Orcus-to-Vanth relative position (Table 1). Orcus ephemeris is based on direct images of the system; thus, it represents the photocentre motion in the sky. To have the correct relative position, we used Equation A.13 from [46], considering the aforementioned expected relative position of 0.24 ± 0.01 arcsec, the expected magnitudes 19.05 ± 0.01 for Orcus and 21.4 ± 0.1 for Vanth, to compute the relative fluxes. This resulted in a photocentre offset on the position of Orcus in the direction to Vanth of 0.023 ± 0.003 arcsec. The corrected relative position, accounting for the main body uncertainty, is presented in Appendix A, Table 9.

Solution	Date and Time (UT) Julian date	Right ascension (h m s) Declination ($^{\circ}$ ' ")	Offset (X, Y) (km)	Uncertainty (km)
North	2014-03-01 16:19:01.120	09 58 22.55266 \pm 0.19	2760.8	6.3
	2456718.1798740742	-08 16 55.1837 \pm 0.116	6530.1	3.8
South	2014-03-01 16:19:01.120	09 58 22.55234 \pm 0.20	2600.5	6.8
	2456718.1798740742	-08 16 55.19536 \pm 0.087	6133.0	2.8

Table 1. Vanth's ICRS position for each possible solution, i.e., body centre to the North or South of the chord, for the event date, time and an object distance of 47.08 au. The propagated Gaia DR3 star position is RA: 09h 58m 22.54817s \pm 0.0302 mas, DEC: $-08^{\circ} 16' 55''.34010 \pm 0.0315$ mas. The uncertainties of Vanth's Right Ascension and Declination ($\Delta\alpha(\cos\delta)$, $\Delta\delta$) are given in mas. The offset position (X, Y) of Vanth is given in the tangent plane aligned with the equatorial coordinates with respect to the main body ephemeris (NIMAv10). Contrarily to Table 9, the 1σ uncertainties on (X, Y) are based here only on the expected satellite diameter, assumed to be spherical, fitted to the observed occultation chord.

(ii) March 07, 2017

The occultation by Vanth on March 07, 2017, involved a (previously unknown) binary star. The event was fortuitously detected from two sites, and high-resolution images of the target star provided subsequently their positions relative to the photocentre of the system, see details in [28]. The authors used astrometric positions obtained the night of the occultation to calculate the Orcus-Vanth system position relative to the bright star and verified that the obtained value agrees with the detected occultation. With that, they derived an Orcus-Vanth relative position of $\Delta\alpha(\cos\delta) = -0.0445 \pm 0.010$ arcsec and $\Delta\delta = -0.2362 \pm 0.001$ arcsec. We have also corrected the relative position by the photocentre offset in the Orcus-Vanth direction by 0.018 ± 0.002 arcsec to derive the (X, Y) positions provided in Appendix A, Table 9.

Using the reported times and the stars' photocentre, we calculated the satellite's astrometric as well as the relative to Orcus position considering NIMAv10 ephemeris (Table 2).

Solution	Date and Time (UT) Julian date	Right ascension (h m s) Declination ($^{\circ}$ ' ")	Offset (X, Y) (km)	Uncertainty (km)
Photocentre	2017-03-07 06:56:37.440	10 08 18.547109 \pm 0.76	-1618.8	1.7
	2457819.7893222221	-09 40 14.010687 \pm 0.46	-6921.5	2.7

Table 2. Similar to Table 1, but for the occultation of 2017. The satellite position considers the binary star's photocentre, RA = 10h 08m 18.54297 s \pm 0.76 mas; DEC = $-09^{\circ} 40' 14''.14747 \pm 0.46$ mas (see text and [28]). The offset (X, Y) is based on the NIVAv10 ephemeris, i.e., the system photocentre. The object was at a geocentric distance of 47.14 au.

(iii) Orbital elements

Using GENOID, the aforementioned occultation-derived positions, and 14 relative positions from high-resolution images [48–50], we obtained pure Keplerian orbits of Vanth around Orcus. Both mirrored, prograde and retrograde solutions are presented in Table 3, where the prograde presents smaller χ^2 per degree of freedom (χ_{pdf}^2)¹⁰. The 2014 point has a residual of almost 30 mas, which is partially responsible for a χ_{pdf}^2 significantly larger than the unity and may be caused by either a systematic error in Orcus' ephemeris, a timing issue on the data, a non-circular apparent limb, or, most probably, a combination of these. The low uncertainties of the 2006 HST data points and 2016 observations from ALMA are also contributing to the increase in the χ_{pdf}^2 . All this data obtained from different sources, imaging, stellar occultation and millimetres, have proved to be difficult to analyse in a consistent way, as they may have different sources of systematic errors. The χ^2 plots for some orbital elements are provided in Appendix B.

These results can be compared with previously published values [24,42,50,52]. The retrograde solution is comparable to the solutions presented by [24]. Both solutions are consistent with a circular motion. If we assume the orbit became circularized, this could have been caused by a physical mechanism, such as tidal forces, friction with particles composing a dust ring, possibly during the satellite's own accretion, or gravitational interaction with another (unknown) satellite. Differently from [42], our non-Keplerian solution does not improve the quality of the fit, so we do not fit the J_2 factor. This difference may come from the algorithms' different capabilities for exploring the space parameters. Figure 3 presents the prograde orbit of Vanth around Orcus projected in the sky plane, while Figure 4 presents the retrograde orbit of Vanth.

Vanth (Orcus/1)							
Orbital elements EQJ2000			Derived parameters			Observing data set	
Prograde							
P (days)	9.53894	± 0.00010	Syst. mass	6.163	± 0.079	N. Obs.	14
a (km)	8912	± 38	($\times 10^{20}$ kg)			N. Occ.	2
e	0.0010	< 0.0030	α_p ($^\circ$)	327.0	± 2.1	Time span	4132 days
i ($^\circ$)	66.4	± 1.8	δ_p ($^\circ$)	23.62	± 0.85	1 st date	2005-11-12
Ω ($^\circ$)	57.0	± 2.1	λ_p ($^\circ$)	338.3	± 2.2	RMS (mas)	6.9
ω ($^\circ$)	158.4	± 7.0	β_p ($^\circ$)	34.20	± 0.92	χ_{pdf}^2	7.0
t_p (JD)	2455994.27	± 0.19					
Retrograde							
P (days)	9.5391320	± 0.00008	Syst. mass	6.92413	± 0.00035	N. Obs.	14
a (km)	9264.33	± 0.13	($\times 10^{20}$ kg)			N. Occ.	2
e	0.0000	< 0.00073	α_p ($^\circ$)	323.9	± 2.0	Time span	4132 days
i ($^\circ$)	109.13	± 0.63	δ_p ($^\circ$)	-19.13	± 0.63	1 st date	2005-11-12
Ω ($^\circ$)	53.9	± 2.0	λ_p ($^\circ$)	320.0	± 1.8	RMS (mas)	7.3
ω ($^\circ$)	126.3	± 1.9	β_p ($^\circ$)	-5.00	± 0.69	χ_{pdf}^2	15.5
t_p (JD)	2455993.450	± 0.048					

Table 3. Vanth's orbital elements centred at Orcus, expressed in Equatorial J2000: orbital period P , semi-major axis a , eccentricity e , inclination i , the longitude of the ascending node Ω , the argument of pericentre ω , time of passage at pericentre t_p in Julian date. The system total mass M , the Equatorial J2000 coordinates (α_p , δ_p) and the Ecliptic J2000 coordinates of the orbital pole (λ_p , β_p) are provided. Finally, the number of relative positions from direct images and the number of positions from stellar occultations, the period between the observations, the date of the first used observation, and the dispersion of the data with respect to the fitted orbit are also provided. Uncertainties are given at 1σ .

¹⁰The much smaller uncertainties on the orbital parameters of the retrograde solution, when compared to the prograde solution, is an indication that the solution was trapped in a local minimum, i.e. any deviation from that value results in a degenerate fit, as can be noticed in Figure 7, top left panel.

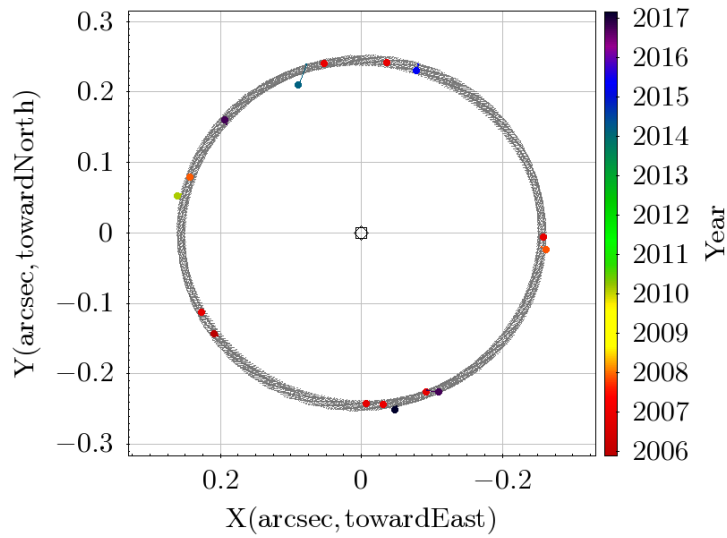


Figure 3. Vanth's orbit around Orcus projected in the sky plane. The data points are coloured according to the observation year. The calculated orbit is indicated by grey points, and its thickness stems from the changing viewing geometry between 2005 and 2017. The small segments connect the observed positions to the calculated solution. Even if the 2014 occultation point (in purple) has been corrected by the photocentric shift, it is still off the orbit solution, augmenting the χ^2_{pdf} value of the fit.

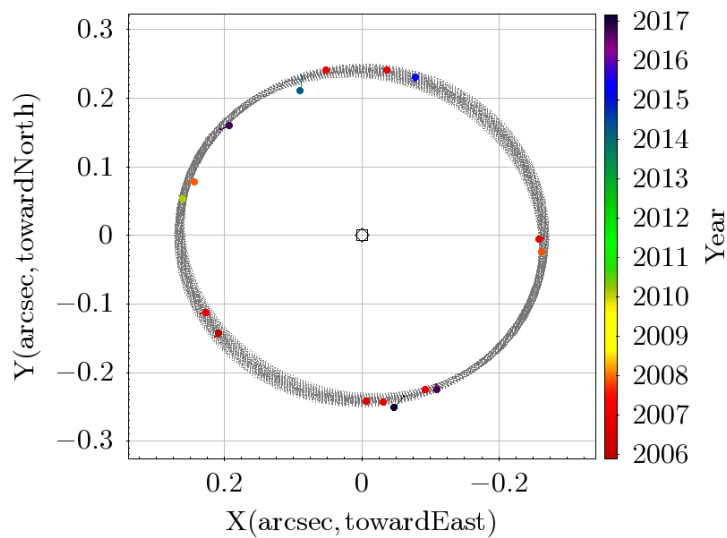


Figure 4. Similar as Figure 3 but for the retrograde solution of Vanth's orbit around Orcus projected in the sky plane.

(b) Weywot (Quaoar/1)

Quaoar is one of the largest Trans-Neptunian Objects orbiting in the Hot Classical region with a semi-major axis of 43.5 au, a small eccentricity of 0.041, and an orbital inclination of 8.0 degrees. It has an equivalent diameter of 1110 ± 10 km, measured with a stellar occultation in 2011 under the assumption of a Maclaurian shape [11]. In 2023, two rings were announced around Quaoar [13,14] at distances of about 2500 km and 4000 km, well outside the classical Roche limit, estimated to be at less than 1800 km from Quaoar's centre [13]. The outermost ring is inhomogeneous and very

close to the 1/3 spin-orbit resonance with Quaoar, considering the rotation period of ~ 17.7 hours, which is the case for a triaxial object [53].

Its moon, Weywot, was found in 2006 [54], and had its diameter estimated to be 81 ± 11 km, based on thermal data, under the assumption of equal albedo relative to Quaoar of $12 \pm 1\%$ [55]. Its orbital semi-axis is on the order of 13300 km with a period of ~ 12.4 days.

Several attempts to detect stellar occultations by Weywot have been made by our team since 2012, but the first detection made in 2019 was a lucky catch, with both Quaoar and Weywot in the same light curve. With the preliminary relative position obtained from that event, we used GENOID to update the orbital fit and calculated its ephemeris, which was available through IMCCE's *Miriade* service.

Using NIMA ephemeris for Quaoar and GENOID ephemeris for the relative position of Weywot, we predicted and successfully detected occultations by Weywot in June 2022 and 2023, crossing the USA, as well as an event in May 2023, crossing New Zealand. Although the detailed analysis of these events is the subject of a work in development, all of them are consistent with a circular limb fit with a diameter of ~ 170 km, significantly larger than the thermally-derived value 81 ± 11 km mentioned earlier [55], which indicates a much darker surface when compared to Quaoar's. In this work, we assume a spherical shape with a 170-km diameter to derive Weywot's position relative to Quaoar.

Quaoar's NIMAv19 ephemeris is based on astrometric positions obtained from about 20 stellar occultations detected from 2011 up to 2024, as well as MPC and proprietary classical astrometric positions. Due to the much better accuracy and weight given to the occultation derived positions, the ephemeris is dominated by these positions, thus, it is not affected by the photocentre displacement caused by the satellite present on the direct unresolved image. Therefore we do not correct Weywot's relative positions reported here from the photocentre offset, as NIMAv19 already provides the primary body centre of figure position.

(i) August 04, 2019

An occultation by Quaoar was predicted to cross Namibia on August 04, 2019. Observations were attempted from the Tivoli site. Thankfully, the observer started to acquire data fourteen minutes before the predicted time, registering the occultation by Weywot eleven minutes before the Quaoar event.

Quaoar's chord had a length of 1121 ± 15 km; thus, it is very close to being diametric. From this observation, we derived the astrometric position of Quaoar presented in table 4. Using the diameter of 170 km (as explained above), we can fit two circles to the single 168 ± 15 km observed chord. One solution has the circle's centre to the North of the chord, and the other has the centre to the South of it. Both are presented in Table 4. Considering the occulted star, main body, and chord fit, the final relative position (X, Y) and uncertainties are given in Appendix A, table 10.

(ii) June 11, 2022

Using GENOID and NIMA updated ephemeris, which considered the former occultation, this event was predicted to cross the USA. The Occultation Timing Association (IOTA) amateur community was alerted, and observations were also made from Flagstaff facilities. Two positive and one close negative chords were detected on Weywot. Quaoar's shadow crossed the Amazon forest, but no observations could be made.

Although a 20% smaller circle could be used, we fitted a 170 km circle to calculate Weywot's astrometric position (see table 5). NIMAv19 ephemeris uses astrometric positions from several stellar occultations; thus, the uncertainty on its position is of only a couple of mas, i.e., less than 60 km at Quaoar's distance. So, we used NIMAv19 Quaoar's position, not applying any photocentre correction, to calculate Weywot's relative position given in Appendix A, Table 10, where the uncertainty on Quaoar position is considered, as well as the uncertainties stemming from the star position and the circular fit to the chords.

(iii) May 26, 2023

Using the same updated ephemeris as for the 2022 event, we predicted the occultation of Weywot, followed by Quaoar on May 26, 2023, crossing New Zealand and South Australia. Weywot and

Weywot: August 04, 2019 astrometry				
Solution	Date and Time (UT)	Right ascension (h m s)	Offset	Uncertainty
	Julian date	Declination ($^{\circ}$ ' ")	(X, Y) (km)	
Quaoar				
South	2019-08-04 17:24:52.560	18 05 34.78680 \pm 0.37	-22	10
	2458700.2256083335	-15 21 02.068139 \pm 1.38	-19	42
Weywot				
North	2019-08-04 17:24:52.560	18 05 34.75794 \pm 0.27	-12761	8
	2458700.2256083335	-15 21 02.1335 \pm 0.60	-1977	18
South	2019-08-04 17:24:52.560	18 05 34.75795 \pm 0.25	-12757	7
	2458700.2256083335	-15 21 02.1347 \pm 0.62	-2013	19

Table 4. Similar to Table 1, Weywot position relative to Quaoar for each possible solution, i.e., centre to the North or South of the chord. The Quaoar centre was obtained from the limb fitting of the positive chord, considering the propagated Gaia DR3 star position RA: 18h 05m 34.78660s \pm 0.13 mas, DEC: $-15^{\circ} 21' 02''.04630 \pm 0.14$ mas. Weywot's ICRS and (X, Y) position are relative to the obtained Quaoar's centre, not considering the main body uncertainty. Different from Table 10, here, the 1σ uncertainties on (X, Y) consider only the expected satellite diameter fitted to the chord. The object was at a distance of 42.08 au.

Weywot: June 11, 2022 astrometry				
Solution	Date and Time (UT)	Right ascension (h m s)	Offset	Uncertainty
	Julian date	Declination ($^{\circ}$ ' ")	(X, Y) (km)	
Circle	2022-06-11 09:13:52.920	18 26 06.65650 \pm 0.15	-6598.2	1.6
	2459741.8846402778	-15 07 47.33584 \pm 0.15	-3870.2	1.5

Table 5. Similar to Table 1, using the NIMAv19 ephemeris and assuming that Quaoar is centred, considering the propagated Gaia DR3 star position RA: 18h 26m 06.67152s \pm 0.14 mas, DEC: $-15^{\circ} 07' 47''.49461 \pm 0.14$ mas. The 1σ uncertainties on (X, Y) consider Weywot's limb fit only. The object was at a distance of 41.785 au.

Quaoar events were detected from the northmost site in Blenheim/NZ, while Quaoar's was also detected from the other three stations in New Zealand.

The four chords detected on Quaoar allow obtaining a precise astrometric position (Table 6) and thus calculate Weywot's relative position. With a chord length of 180 ± 19 km, due to the uncertainty, two solutions are possible for the object's centre, which are presented in Table 6. Considering the circular fit and the uncertainty on Quaoar's position, the relative offset position is given in Appendix A, Table 10.

(iv) June 22, 2023

The occultation of June 22, 2023, was very similar to that of 2022 and was also detected by IOTA astronomers and Flagstaff facilities. Five positive chords were recorded, and close negatives to the North and South limited the possible solutions. A 170 km circle is compatible with the observed chords, so we fitted the circular limb to derive Weywot's astrometric position (Table 7). NIMAv19 ephemeris was used to calculate the relative position available in Table 10, where the uncertainty on Quaoar position is considered, as well as the star position and the circular fit to the chords.

(v) Orbital elements

Using the four relative positions derived from the detected stellar occultations and nine direct images (see table 10), we calculated Weywot's orbit relative to Quaoar. Using the Keplerian model, we obtained the solution presented in Table 8, where the system mass and the orbital pole are also shown. These results represent a significant improvement in terms of uncertainties from previous works [39,42], with smaller mass and eccentricity and larger semi-major axis. The 2011

Weywot: May 26, 2023 astrometry				
Solution	Date and Time (UT)	Right ascension (h m s)	Offset	Uncertainty
	Julian date	Declination ($^{\circ}$ ' ")	(X, Y) (km)	(km)
Quaoar				
Elliptical	2023-05-26 15:53:06.640	18 32 44.928582 \pm 0.20	49.2	1.4
	2460091.1618824075	-15 03 49.081808 \pm 0.33	11.1	8.0
Weywot				
North	2023-05-26 15:53:06.640	18 32 44.90169 \pm 0.30	-11829.4	7.0
	2460091.1618824075	-15 03 49.0467 \pm 0.48	1066.4	15.5
South	2023-05-26 15:53:06.640	18 32 44.90169 \pm 0.30	-11829.8	7.0
	2460091.1618824075	-15 03 49.0476 \pm 0.48	1039.7	15.7

Table 6. Similar to Table 1, Weywot position relative to Quaoar. A Quaoar centre was obtained from the limb fitting of the four positive chords. The ICRS positions consider the propagated Gaia DR3 star position RA: 18h 32m 44.92889s \pm 0.19 mas, DEC: -15 $^{\circ}$ 03' 48".97855 \pm 0.19 mas. Weywot's position (X, Y) relative to Quaoar's centre, does not consider the main body uncertainty. The object was at a geocentric distance of 41.8730 au.

Weywot: June 22, 2023 astrometry				
Solution	Date and Time (UT)	Right ascension (h m s)	Offset	Uncertainty
	Julian date	Declination ($^{\circ}$ ' ")	(X, Y) (km)	(km)
Diametrical	2023-06-22 08:00:48.900	18 30 45.75455 \pm 0.35	-11956.1	0.1
	2460117.8338993057	-15 03 33.491764 \pm 0.39	-3420.1	0.8

Table 7. Similar to Table 1, Weywot position relative to Quaoar using the NIMAv19 ephemeris and assuming that Quaoar is centred. Considering the propagated Gaia DR3 star position RA: 18h 30m 45.78240s \pm 0.35 mas, DEC: -15 $^{\circ}$ 03' 33".64224 \pm 0.39 mas. The object was at a geocentric distance of 41.7151 au. The uncertainties on (X, Y) only consider the fit to the object limb.

observations made with Keck [56] present systematic negative differences with respect to our solution, with values that reach 14 mas. This may explain the significant differences between our solution and those that do not rely on occultation-derived relative positions.

The Figure 5 displays Weywot's orbit around Quaoar. The χ^2 dependence on some orbital elements can be seen in Appendix B, Figure 8.

The mass, period, and eccentricity are fundamental parameters that eventually inform us about the density of the central body and the possible dynamical link between Weywot and Quaoar's rings. We note in particular that the currently measured pole of Quaoar's main ring Q1R ($\alpha_{Q1R} = 259.8^{\circ} \pm 0.2^{\circ}$, $\delta_{Q1R} = 53.5^{\circ} \pm 0.3^{\circ}$ [14]) presents a difference of $4.8^{\circ} \pm 1.6^{\circ}$ relative to the Weywot's orbital pole given in Table 8, suggesting a possible mutual inclination between Weywot and Q1R. Nevertheless, it is important to consider that this may come from an unknown systematic error on the ring pole determination or from the assumption that it is circular and equatorial to Quaoar.

4. Discussion and Future Prospects

The study of the Outer Solar System using stellar occultation started with observing Pluto events in the 80's (see [57,58] and the review by [9]), but it has been generally applied to other small bodies since 2009 [59]. Since then, numerous interesting results have allowed a deeper understanding of this region [9].

In the era of LSST (Legacy Survey of Space and Time) and the Extremely Large Telescopes, the field will make another significant step toward studying the Transneptunian Binaries. The LSST will discover and repeatedly observe tens of thousands of TNOs, up to \sim 24th magnitude, providing accurate astrometric positions. This will lead to better orbit computations, allowing

Weywot (Quaoar/1)							
Orbital elements EQJ2000			Derived parameters			Observing data set	
P (days)	12.431013	± 0.00021	Syst. mass	1.208	± 0.063	N. Obs.	9
a (km)	13309	± 231	($\times 10^{21}$ kg)			N. Occ.	4
e	0.018	± 0.016	α_p ($^\circ$)	266.9	± 1.5	Time span	6336 days
i ($^\circ$)	38.04	± 1.4	δ_p ($^\circ$)	51.9	± 1.4	1 st date	2006-02-14
Ω ($^\circ$)	356.9	± 1.5	λ_p ($^\circ$)	262.8	± 3.3	RMS (mas)	4.3
ω ($^\circ$)	292	± 25	β_p ($^\circ$)	74.6	± 1.4	χ_{pdf}^2	0.47
t_p (JD)	2453780.42	± 0.82					

Table 8. Same as Table 3 but for Quaoar's satellite, Weywot. Uncertainties are given at 1σ

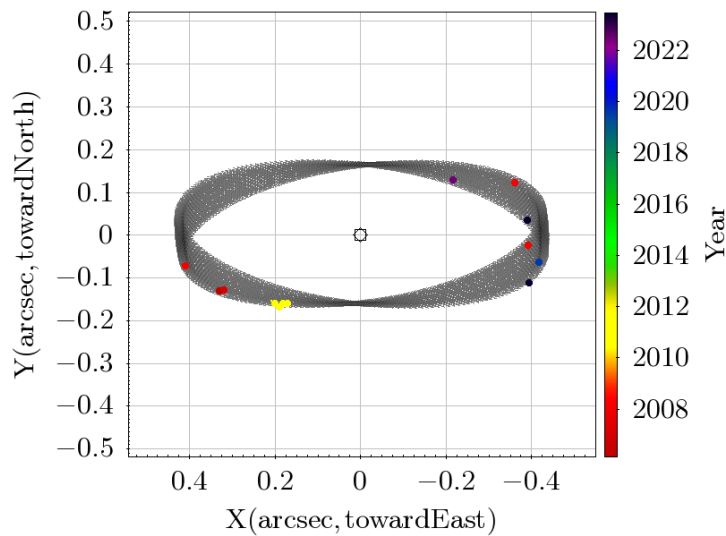


Figure 5. The same as Fig. 3 for Weywot's orbit around Quaoar. The grey points are now significantly spread out due to the changing viewing geometry of Weywot's orbit between 2006 and 2023.

reliable predictions of stellar occultations and enabling an efficient occultation survey for the search of TNOBs on smaller objects. The future extremely large telescopes will be capable of providing direct images with resolutions better than ten milli-arcseconds (mas) with a contrast of 10^{-8} in flux between quite close different sources. This will allow more observations of the TNO satellites, providing further constraints on their composition and rotation period. It will also offer relative positions that will be used to update their orbits, allowing better predictions of occultations by the satellites¹¹.

Stellar occultations now have the capacity to provide km-level sensitivities for both the shape and the on-sky positions of small objects of the outer Solar System [9]. They also allow us to probe the surroundings of these objects, especially the Cold Classicals, searching for small satellites or binary pairs. Using the Earth as a big telescope, thanks to the Pro-Am collaborative work, it will be possible to perform surveys for determining better the number of binary objects below the resolving power of the current telescopes (~ 1200 km), which will be an essential step in understanding solar system formation.

The probability of detecting a pair of objects will depend on their sizes, relative distance, prediction uncertainty and number of telescopes observing the event. Considering that LSST single epoch images will typically deliver astrometric positions with uncertainties of 10 mas, the

¹¹The LineA Occultation Prediction Database was built to provide predictions of all Small Solar System Objects in the LSST era: <https://solarsystem.linea.org.br/>.

TNO ephemeris will have similar precision on short-term predictions (i.e., a few years) [45]. Let us consider that we will want to use an occultation to scan about two thousand kilometres to probe the high-resolution images' blind region, plus the prediction uncertainty. If each component of the binary system have 50 km in diameter, we will want a fence like distribution perpendicular to the shadow path of, at least, one telescope every 25 km, to guarantee the detection. This corresponds to a total of 80 telescopes along the 2000 km region. This may seem to be a large number, but when observing campaigns can count on the collaboration of the amateur community, a large number of telescopes can be involved, as has been the case on the occultations by Triton [60] and 2002 MS₄ [17].

Regarding the satellites, the new Extremely Large telescopes with direct imaging power of a few mas [61], that is, a few hundred kilometres at the TNO distance, will enable more observations of the close environment of the big TNOs and thus their satellites. With more relative positions, better orbits and ephemerides will be calculated.

We have shown that with GENOID plus NIMA, we can provide reliable predictions of stellar occultations by TNO moons as soon as relative positions with sufficiently good quality are available. With the detection of these events from multiple sites, their physical properties can be obtained. As explained in Section 1, information such as shape, albedo, and density allows for a better understanding of their formation history, constraining the Solar System's dynamical evolution scenarios.

GENOID allows for a complete exploration of the orbital space parameters, finding Keplerian solutions for most systems. It also allows studying the influence of the main body's gravitational field perturbations caused by its oblateness and the mutual influence of multiple satellites in the system. A better ephemeris enables the improvement of dynamical studies on resonances, tides, and implications for ring dynamics and confinement [62].

We found that when only the satellite is detected during a stellar occultation, and the main body's ephemeris is based mainly on direct images, it is important to correct its relative position from the photocentric offset caused by the satellite. Conversely, in the case of Quaoar, the photocentre offset has no influence, as its ephemeris is dominated by positions derived from previous stellar occultations.

We have shown that the Orcus-Vanth and Quaoar-Weywot orbital solutions are consistent with purely Keplerian motions. New orbital parameters and masses were obtained, fundamental information for the study of the dynamical environment (e.g. search for stable regions) and for determining the central object's physical properties, such as its density. The new ephemeris will allow for better prediction of future stellar occultations for the full characterization of these satellites and possibly better constraining their origin scenarios.

This work presents a list of all the TNO satellites (excepted Charon) that were successfully detected so far using stellar occultations, and discusses the implications of this starting field of research. It will undoubtedly grow and provide significant results, allowing us to understand better the history of solar system formation.

Acknowledgements. This study was financed in part by the Coordenação de Aperfeiçoamento de Pessoal de Nível Superior - Brasil (CAPES) - Finance Code 001 and National Institute of Science and Technology of the e-Universe project (INCT do e-Universo, CNPq grant 465376/2014-2). FBR acknowledges CNPq grant 316604/2023-2. GM acknowledges the CAPES scholarship number 88887.705245/2022-00. The ephemeris calculations of the position of the bodies of the Solar System were carried out by the IMCCE ephemeris calculation service through its Solar System portal (<https://ssp.imcce.fr>). We thank the observers who reported the observations used in this work and are co-authors of the respective works, yet to be published, with the complete analysis of these events.

A. Satellite positions

The positions taken from the literature used on our orbital fit with GENOID are given in Table 9 for Vanth (Orcus/1) and Table 10 for Weywot (Quaoar/1).

Vanth offset positions relative to Orcus					
Observation Date	X (")	Y (")	X_{err} (")	Y_{err} (")	Source (Ref.)
2005-11-13T03:56:09.600	0.20792	-0.14342	0.00492	0.00992	HST [49]
2006-10-31T20:51:21.600	0.22597	-0.11307	0.00102	0.00071	HST [49]
2006-11-03T01:36:14.184	-0.09310	-0.22635	0.00050	0.00050	HST [49]
2006-11-04T20:47:02.400	-0.25893	-0.00560	0.00050	0.00079	HST [49]
2006-11-12T01:53:45.600	-0.00694	-0.24344	0.00185	0.00050	HST [49]
2006-11-16T14:08:09.600	-0.03718	0.24113	0.00058	0.00050	HST [49]
2006-11-26T15:30:14.400	0.05228	0.24033	0.00085	0.00050	HST [49]
2006-12-10T20:03:50.400	-0.03180	-0.24410	0.00050	0.00050	HST [49]
2007-11-11T19:01:55.200	-0.26300	-0.02400	0.00500	0.00500	HST [49]
2007-12-05T06:43:12.000	0.24288	0.07814	0.00241	0.00418	HST [49]
2010-02-23T05:41:04.704	0.26000	0.05200	0.02500	0.02500	VLT [50]
2014-03-01T16:19:01.120	0.08891	0.21006	0.0082	0.0088	OCC N. [†]
2014-03-01T16:19:01.120	0.08504	0.20690	0.0083	0.0136	OCC S. [†]
2015-04-05T09:07:12.108	-0.07854	0.22974	0.00100	0.00100	Keck [24]
2016-10-11T11:22:40.890	0.1926	0.1596	0.005	0.005	ALMA [48]
2016-10-15T12:05:15.500	-0.1095	-0.2264	0.005	0.005	ALMA [48]
2017-03-07T06:53:51.000	-0.0475	-0.2521	0.011	0.012	OCC [28] [†]

Table 9. Vanth's on-sky offset (X, Y) relative to Orcus and their estimated errors, in arcsec. Occultation-derived (OCC) positions obtained in this work, corrected for the photocentre offset, are marked with '[†]'. The final uncertainty in the quadratic sum of the uncertainties of the Orcus position with the stellar position and the Vanth's radius (222 ± 5 km [28]) to account for its unknown shape.

B. Fitness function

GENOID is a statistical method for minimizing the discrepancies between observed data and the theoretical model. Like the least squares method, this approach is based on the idea that errors follow a normal distribution. The resulting graphs from a GENOID adjustment illustrate the directions of expansion within the parameter space. These graphs are plotted with an adjusted parameter of the dynamic model on the x-axis and the fitness function (labelled as "fp" in the figures), in our case the χ^2 , on the y-axis.

These graphs can present three distinct shapes: a U-shaped curve, a significant slope, or oscillations with local minima. The U-shaped curve indicates that the solution is well-converged. Therefore, small modifications to the initial conditions on either side of the optimal solution result in a degradation of the fit. In the case of oscillations with multiple local minima, it is necessary to explore each possibility by narrowing the search space around each minimum and recalculating to analyse how each restricted system behaves. Generally, the absolute minimum is chosen as the final solution. Finally, when the graphs show a slope, this suggests that the search space must be shifted in the direction that minimizes the χ^2 . The calculations are then repeated until a solution is obtained that produces a U-shaped graph.

Figure 6 shows the curves for Vanth (Orcus/1) prograde solution, while Fig. 7 shows the curves for Vanth (Orcus/1) retrograde solution and Fig. 8 shows the curves for Weywot (Quaoar/1) orbital solution.

References

1. Levison HF, Morbidelli A. 2003 The formation of the Kuiper belt by the outward transport of bodies during Neptune's migration. *Nature* **426**, 419–421. ([10.1038/nature02120](https://doi.org/10.1038/nature02120))
2. Gomes RS, Morbidelli A, Levison HF. 2004 Planetary migration in a planetesimal disk: why did Neptune stop at 30 AU?. *Icarus* **170**, 492–507. ([10.1016/j.icarus.2004.03.011](https://doi.org/10.1016/j.icarus.2004.03.011))
3. Tsiganis K, Gomes R, Morbidelli A, Levison HF. 2005 Origin of the orbital architecture of the giant planets of the Solar System. *Nature* **435**, 459–461. ([10.1038/nature03539](https://doi.org/10.1038/nature03539))

Weywot offset positions relative to Quaoar

Observation Date	X (")	Y (")	X_{err} (")	Y_{err} (")	Source (Ref.)
2006-02-14T21:30:32.940	0.3288	-0.1311	0.00797	0.00253	HST [56]
2007-03-19T15:22:58.512	0.3177	-0.1288	0.00188	0.00264	HST [56]
2008-03-10T04:55:31.980	-0.3922	-0.0251	0.00396	0.00363	HST [56]
2008-03-15T01:31:01.992	0.4082	-0.0721	0.00371	0.00144	HST [56]
2008-03-20T16:28:01.992	-0.3622	0.1230	0.00332	0.00370	HST [56]
2011-06-07T07:53:07.584	0.1700	-0.1600	0.01000	0.01000	Keck [56]
2011-06-07T09:32:12.768	0.1800	-0.1600	0.01000	0.01000	Keck [56]
2011-06-07T10:58:56.640	0.1900	-0.1700	0.01000	0.01000	Keck [56]
2011-06-07T12:25:19.776	0.2000	-0.1600	0.01000	0.01000	Keck [56]
2019-08-04T17:24:52.560	-0.41820	-0.06476	0.0028	0.0032	OCC N. [†]
2019-08-04T17:24:52.560	-0.41797	-0.06596	0.0028	0.0031	OCC S. [†]
2022-06-11T09:13:52.920	-0.2177	0.1277	0.0035	0.0031	OCC †
2023-05-26T15:53:06.640	-0.38953	0.03512	0.0028	0.0029	OCC N. [†]
2023-05-26T15:53:06.640	-0.38952	0.03424	0.0028	0.0029	OCC S. [†]
2023-06-22T08:00:48.900	-0.3952	-0.1130	0.0035	0.0030	OCC †

Table 10. The same as Table 9 for Weywot's position relative to Quaoar. Detailed analyses of the stellar occultation results will be presented in future work. The June 2022 and 2023 results are based on the NIMAv19 position of Quaoar, which has an estimated uncertainty of $\sigma_{\alpha}(\cos \delta) = 2.0$ mas and $\sigma_{\delta} = 1.0$ mas for both events. The final uncertainty is the quadratic sum of Quaoar's position with the stellar position and the Weywot's radius (85 km)(assumed spherical), to account for its unknown shape. Conversely, the 2019 and May 2023 events have smaller uncertainties, as Quaoar was also detected, providing more accurate relative positions.

4. Nesvorný D, Vokrouhlický D. 2016 Neptune's Orbital Migration Was Grainy, Not Smooth. *ApJ* **825**, 94. ([10.3847/0004-637X/825/2/94](https://doi.org/10.3847/0004-637X/825/2/94))
5. Gladman B, Marsden BG, Vanlaerhoven C. 2008 Nomenclature in the Outer Solar System. In Barucci MA, Boehnhardt H, Cruikshank DP, Morbidelli A, Dotson R, editors, *The Solar System Beyond Neptune*, pp. 43–57. University of Arizona Press.
6. Gladman B, Volk K. 2021 Transneptunian Space. *ARA&A* **59**, 203–246. ([10.1146/annurev-astro-120920-010005](https://doi.org/10.1146/annurev-astro-120920-010005))
7. Parker AH, Kavelaars JJ. 2010 Destruction of Binary Minor Planets During Neptune Scattering. *ApJ* **722**, L204–L208. ([10.1088/2041-8205/722/2/L204](https://doi.org/10.1088/2041-8205/722/2/L204))
8. Thirouin A, Sheppard SS. 2019 Light Curves and Rotational Properties of the Pristine Cold Classical Kuiper Belt Objects. *AJ* **157**, 228. ([10.3847/1538-3881/ab18a9](https://doi.org/10.3847/1538-3881/ab18a9))
9. Sicardy B, Braga-Ribas F, Buie MW, Ortiz JL, Roques F. 2024 Stellar occultations by trans-Neptunian objects. *The Astronomy and Astrophysics Review* **32**, 6. ([10.1007/s00159-024-00156-x](https://doi.org/10.1007/s00159-024-00156-x))
10. Ortiz JL, Sicardy B, Camargo JIB, Santos-Sanz P, Braga-Ribas F. 2020 Stellar occultation by TNOs: from predictions to observations. In Prialnik D, Barucci MA, Young L, editors, *The Trans-Neptunian Solar System*, pp. 413–437. Elsevier. ([10.1016/B978-0-12-816490-7.00019-9](https://doi.org/10.1016/B978-0-12-816490-7.00019-9))
11. Braga-Ribas F, Sicardy B, Ortiz JL, Lellouch E, Tancredi G, Lecacheux J, Vieira-Martins R, Camargo JIB, Assafin M, Behrend R, Vachier F, Colas F, Morales N, Maury A, Emilio M, Amorim A, Unda-Sanzana E, Roland S, Bruzzone S, Almeida LA, Rodrigues CV, Jacques C, Gil-Hutton R, Vanzi L, Milone AC, Schoenell W, Salvo R, Almenares L, Jehin E, Manfroid J, Sposetti S, Tanga P, Klotz A, Frappa E, Cacella P, Colque JP, Neves C, Alvarez EM, Gillon M, Pimentel E, Giacchini B, Roques F, Widemann T, Magalhães VS, Thirouin A, Duffard R, Leiva R, Toledo I, Capeche J, Beisker W, Pollock J, Cedeño Montaña CE, Ivarsen K, Reichart D, Haislip J, Lacluyze A. 2013 The Size, Shape, Albedo, Density, and Atmospheric Limit of Transneptunian Object (50000) Quaoar from Multi-chord Stellar Occultations. *ApJ* **773**, 26. ([10.1088/0004-637X/773/1/26](https://doi.org/10.1088/0004-637X/773/1/26))
12. Ortiz JL, Santos-Sanz P, Sicardy B, Benedetti-Rossi G, Bérard D, Morales N, Duffard R, Braga-Ribas F, Hopp U, Ries C, Nascimbeni V, Marzari F, Granata V, Pál A, Kiss C, Pribulla T, Komžík

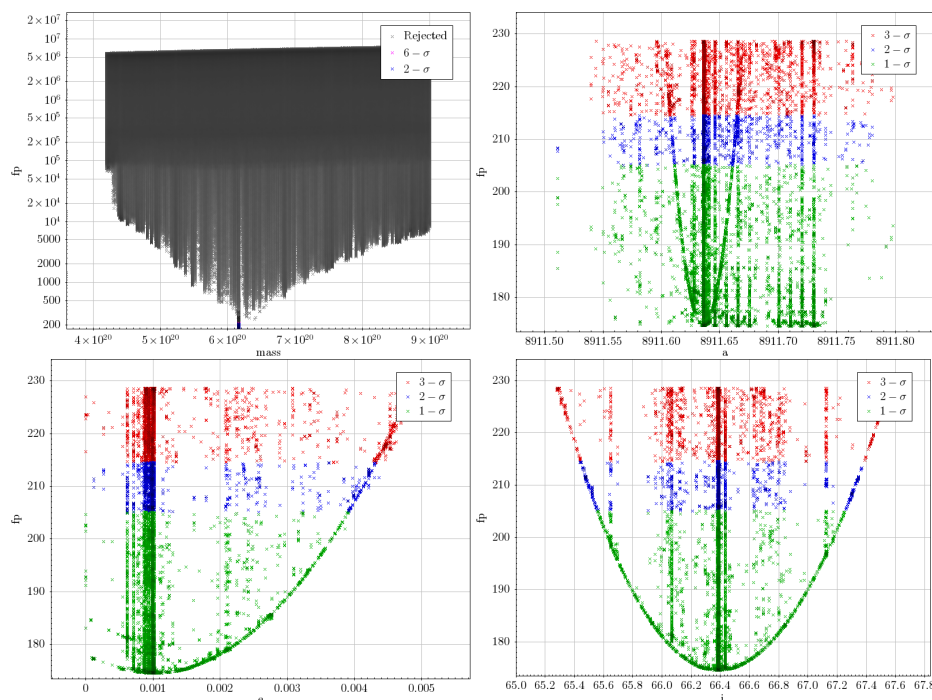


Figure 6. The χ^2 values are plotted versus some of the fitted parameters for the prograde solution of Vanth's orbit around Orcus. The top left panel presents all the space of parameters explored for the fit of the system mass, showing a well-defined minimum. The top right panel shows the 1 to 3σ regions for the semi-major axis a . The bottom left and right panels show the same for the orbital eccentricity e and inclination i , respectively. The eccentricity for the prograde solution has its minimum close to, but not at zero, although the circular solution cannot be discarded.

- R, Hornoch K, Pravec P, Bacci P, Maestripieri M, Nerli L, Mazzei L, Bachini M, Martinelli F, Succi G, Ciabattari F, Mikuz H, Carbognani A, Gaehrken B, Mottola S, Hellmich S, Rommel FL, Fernández-Valenzuela E, Campo Bagatin A, Cikota S, Cikota A, Lecacheux J, Vieira-Martins R, Camargo JIB, Assafin M, Colas F, Behrend R, Desmars J, Meza E, Alvarez-Candal A, Beisker W, Gomes-Junior AR, Morgado BE, Roques F, Vachier F, Berthier J, Mueller TG, Madiedo JM, Unsalan O, Sonbas E, Karaman N, Erece O, Koseoglu DT, Ozisik T, Kalkan S, Guney Y, Niaei MS, Satir O, Yesilyaprak C, Puskullu C, Kabas A, Demircan O, Alikakos J, Charmandaris V, Leto G, Ohlert J, Christille JM, Szakáts R, Takácsné Farkas A, Varga-Verebélyi E, Marton G, Marciniak A, Bartczak P, Santana-Ros T, Butkiewicz-Bak M, Dudziński G, Alí-Lagoa V, Gazeas K, Tzouganatos L, Paschalis N, Tsamis V, Sánchez-Lavega A, Pérez-Hoyos S, Hueso R, Guirado JC, Peris V, Iglesias-Marzoa R. 2017 The size, shape, density and ring of the dwarf planet Haumea from a stellar occultation. *Nature* **550**, 219–223. ([10.1038/nature24051](https://doi.org/10.1038/nature24051))
13. Morgado BE, Sicardy B, Braga-Ribas F, Ortiz JL, Salo H, Vachier F, Desmars J, Pereira CL, Santos-Sanz P, Sfair R, de Santana T, Assafin M, Vieira-Martins R, Gomes-Júnior AR, Margoti G, Dhillon VS, Fernández-Valenzuela E, Broughton J, Bradshaw J, Langersek R, Benedetti-Rossi G, Souami D, Holler BJ, Kretlow M, Bouffleur RC, Camargo JIB, Duffard R, Beisker W, Morales N, Lecacheux J, Rommel FL, Herald D, Benz W, Jehin E, Jankowsky F, Marsh TR, Littlefair SP, Bruno G, Pagano I, Brandeker A, Collier-Cameron A, Florén HG, Hara N, Olofsson G, Wilson TG, Benkhaldoun Z, Busuttil R, Burdanov A, Ferrais M, Gault D, Gillon M, Hanna W, Kerr S, Kolb U, Nosworthy P, Sebastian D, Snodgrass C, Teng JP, de Wit J. 2023 A dense ring of the trans-Neptunian object Quaoar outside its Roche limit. *Nature* **614**, 239–243. ([10.1038/s41586-022-05629-6](https://doi.org/10.1038/s41586-022-05629-6))
 14. Pereira CL, Sicardy B, Morgado BE, Braga-Ribas F, Fernández-Valenzuela E, Souami D, Holler BJ, Bouffleur RC, Margoti G, Assafin M, Ortiz JL, Santos-Sanz P, Epinat B, Kervella P, Desmars J, Vieira-Martins R, Kilic Y, Gomes Júnior AR, Camargo JIB, Emilio M, Vara-Lubiano M,

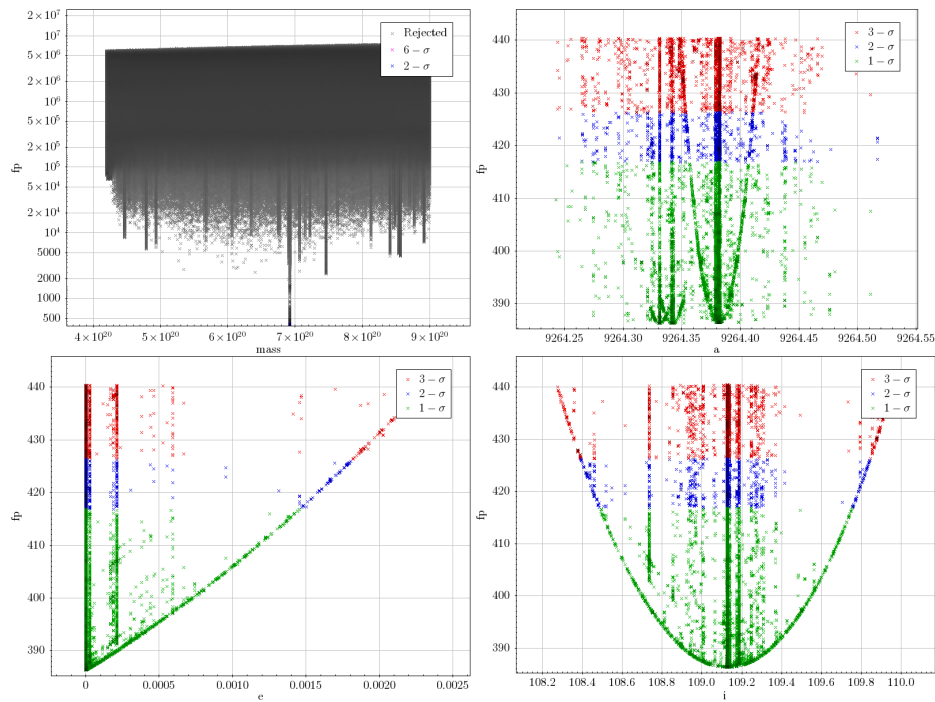


Figure 7. The same as Fig. 6 for the retrograde solution of Vanth's orbit. Again, the top left panel displays a well-defined minimum. The bottom left panel shows that the best retrograde solution is the circular orbit.

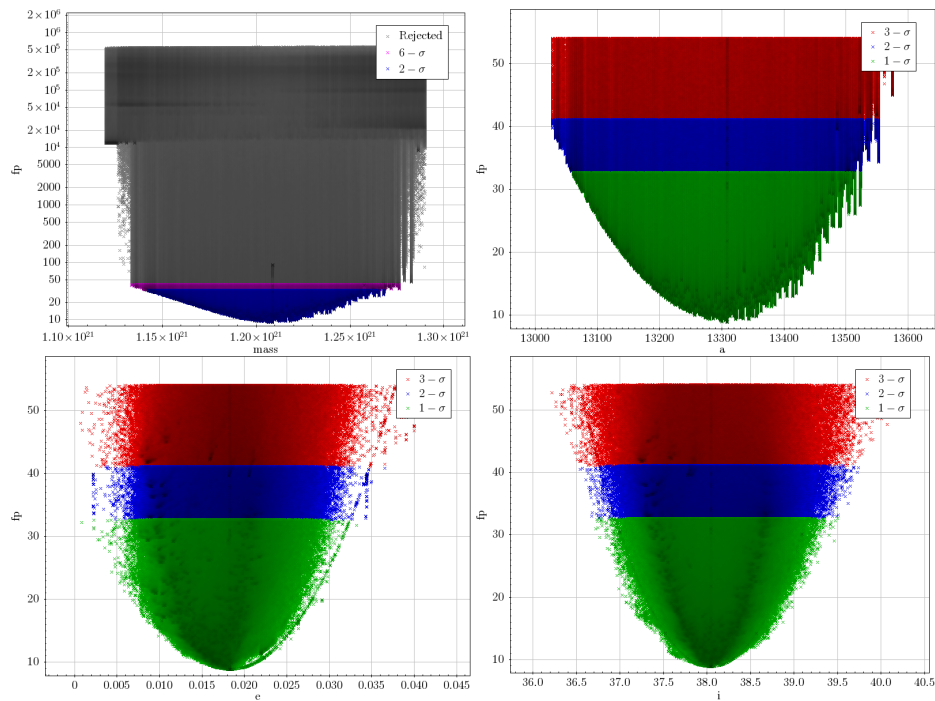


Figure 8. The same as Fig. 6 for the Weywot orbit solution around Quaoar.

- Kretlow M, Albert L, Alcock C, Ball JG, Bender K, Buie MW, Butterfield K, Camarca M, Castro-Chacón JH, Dunford R, Fisher RS, Gamble D, Geary JC, Gnilka CL, Green KD, Hartman ZD, Huang CK, Januszewski H, Johnston J, Kagitani M, Kamin R, Kavelaars JJ, Keller JM, de Kleer KR, Lehner MJ, Luken A, Marchis F, Marlin T, McGregor K, Nikitin V, Nolthenius R, Patrick C, Redfield S, Rengstorf AW, Reyes-Ruiz M, Seccull T, Skrutskie MF, Smith AB, Sproul M, Stephens AW, Szentgyorgyi A, Sánchez-Sanjuán S, Tatsumi E, Verbiscer A, Wang SY, Yoshida F, Young R, Zhang ZW. 2023 The two rings of (50000) Quaoar. *A&A* **673**, L4. ([10.1051/0004-6361/202346365](https://doi.org/10.1051/0004-6361/202346365))
15. Meza E, Sicardy B, Assafin M, Ortiz JL, Bertrand T, Lellouch E, Desmars J, Forget F, Bérard D, Doressoundiram A, Lecacheux J, Oliveira JM, Roques F, Widemann T, Colas F, Vachier F, Renner S, Leiva R, Braga-Ribas F, Benedetti-Rossi G, Camargo JIB, Dias-Oliveira A, Morgado B, Gomes-Júnior AR, Vieira-Martins R, Behrend R, Tirado AC, Duffard R, Morales N, Santos-Sanz P, Jelínek M, Cunniffe R, Querel R, Harnisch M, Jansen R, Pennell A, Todd S, Ivanov VD, Oпитom C, Gillon M, Jehin E, Manfroid J, Pollock J, Reichart DE, Haislip JB, Ivarsen KM, LaCluyze AP, Maury A, Gil-Hutton R, Dhillon V, Littlefair S, Marsh T, Veillet C, Bath KL, Beisker W, Bode HJ, Kretlow M, Herald D, Gault D, Kerr S, Pavlov H, Faragó O, Klös O, Frappa E, Lavayssière M, Cole AA, Giles AB, Greenhill JG, Hill KM, Buie MW, Olkin CB, Young EF, Young LA, Wasserman LH, Devogèle M, French RG, Bianco FB, Marchis F, Brosch N, Kaspi S, Polishook D, Manulis I, Ait Moulay Larbi M, Benkhaldoun Z, Daassou A, El Azhari Y, Moulane Y, Broughton J, Milner J, Dobosz T, Bolt G, Lade B, Gilmore A, Kilmartin P, Allen WH, Graham PB, Loader B, McKay G, Talbot J, Parker S, Abe L, Bendjoya P, Rivet JP, Vernet D, Di Fabrizio L, Lorenzi V, Magazzú A, Molinari E, Gazeas K, Tzouganatos L, Carbognani A, Bonnoli G, Marchini A, Leto G, Sanchez RZ, Mancini L, Kattentidt B, Dohrmann M, Guhl K, Rothe W, Walzel K, Wortmann G, Eberle A, Hampf D, Ohlert J, Krannich G, Murawsky G, Gährken B, Gloistein D, Alonso S, Román A, Communal JE, Jabet F, deVisscher S, Sérot J, Janik T, Moravec Z, Machado P, Selva A, Perelló C, Rovira J, Conti M, Papini R, Salvaggio F, Noschese A, Tsamis V, Tigani K, Barroy P, Irzyk M, Neel D, Godard JP, Lanoiselée D, Sogorb P, Vérilhac D, Bretton M, Signoret F, Ciabattari F, Naves R, Boutet M, De Queiroz J, Lindner P, Lindner K, Enskonatus P, Dangl G, Tordai T, Eichler H, Hattenbach J, Peterson C, Molnar LA, Howell RR. 2019 Lower atmosphere and pressure evolution on Pluto from ground-based stellar occultations, 1988-2016. *A&A* **625**, A42. ([10.1051/0004-6361/201834281](https://doi.org/10.1051/0004-6361/201834281))
 16. Dias-Oliveira A, Sicardy B, Ortiz JL, Braga-Ribas F, Leiva R, Vieira-Martins R, Benedetti-Rossi G, Camargo JIB, Assafin M, Gomes-Júnior AR, Baug T, Chandrasekhar T, Desmars J, Duffard R, Santos-Sanz P, Ergang Z, Ganesh S, Ikari Y, Irawati P, Jain J, Liying Z, Richichi A, Shengbang Q, Behrend R, Benkhaldoun Z, Brosch N, Daassou A, Frappa E, Gal-Yam A, Garcia-Lozano R, Gillon M, Jehin E, Kaspi S, Klotz A, Lecacheux J, Mahasena P, Manfroid J, Manulis I, Maury A, Mohan V, Morales N, Ofek E, Rinner C, Sharma A, Sposetti S, Tanga P, Thirouin A, Vachier F, Widemann T, Asai A, Hayato W, Hiroyuki W, Owada M, Yamamura H, Hayamizu T, Bradshaw J, Kerr S, Tomioka H, Andersson S, Dangl G, Haymes T, Naves R, Wortmann G. 2017 Study of the Plutino Object (208996) 2003 AZ₈₄ from Stellar Occultations: Size, Shape, and Topographic Features. *AJ* **154**, 22. ([10.3847/1538-3881/aa74e9](https://doi.org/10.3847/1538-3881/aa74e9))
 17. Rommel FL, Braga-Ribas F, Ortiz JL, Sicardy B, Santos-Sanz P, Desmars J, Camargo JIB, Vieira-Martins R, Assafin M, Morgado BE, Bouffleur RC, Benedetti-Rossi G, Gomes-Júnior AR, Fernández-Valenzuela E, Holler BJ, Souami D, Duffard R, Margoti G, Vara-Lubiano M, Lecacheux J, Plouvier JL, Morales N, Maury A, Fabrega J, Ceravolo P, Jehin E, Albanese D, Mariey H, Cikota S, Ruždjak D, Cikota A, Szakáts R, Baba Aissa D, Gringahcene Z, Kashuba V, Koshkin N, Zhukov V, Fişek S, Çakir O, Özer S, Schnabel C, Schnabel M, Signoret F, Morrone L, Santana-Ros T, Pereira CL, Emilio M, Burdanov AY, de Wit J, Barkaoui K, Gillon M, Leto G, Frasca A, Catanzaro G, Sanchez RZ, Tagliaferri U, Di Sora M, Isopi G, Krugly Y, Slyusarev I, Chiorny V, Mikuž H, Bacci P, Maestripieri M, Grazia MD, de la Cueva I, Yuste-Moreno M, Ciabattari F, Kozhukhov OM, Serra-Ricart M, Alarcon MR, Licandro J, Masi G, Bacci R, Bosch JM, Behem R, Prost JP, Renner S, Conjat M, Bachini M, Succi G, Stoian L, Juravle A, Carosati D, Gowe B, Carrillo J, Zheleznyak AP, Montigiani N, Foster CR, Mannucci M, Ruocco N, Cuevas F, Di Marcantonio P, Coretti I, Iafrate G, Baldini V, Collins M, Pál A, Csák B, Fernández-García E, Castro-Tirado AJ, Hudin L, Madiedo JM, Anghel RM, Calvo-Fernández JF, Valvasori A, Guido E, Gherase RM, Kamoun S, Fafet R, Sánchez-González M, Curelaru L, Vîntdevară CD,

- Danescu CA, Gout JF, Schmitz CJ, Sota A, Belskaya I, Rodríguez-Marco M, Kilic Y, Frappa E, Klotz A, Lavayssière M, Oliveira JM, Popescu M, Mammata LA, Fernández-Lajús E, Schmidt M, Hopp U, Komžík R, Pribulla T, Tomko D, Husárik M, Erece O, Eryilmaz S, Buzzi L, Gährken B, Nardiello D, Hornoch K, Sonbas E, Er H, Burwitz V, Sybilski PW, Bykowski W, Müller TG, Ogloza W, Gonçalves R, Ferreira JF, Ferreira M, Bento M, Meister S, Bagiran MN, Tekeş M, Marciniak A, Moravec Z, Delinčák P, Gianni G, Casalnuovo GB, Boutet M, Sanchez J, Klemm B, Wuensche N, Burzynski W, Borkowski M, Serrau M, Dangl G, Klös O, Weber C, Urbaník M, Rousselot L, Kubánek J, André P, Colazo C, Spagnotto J, Sickafoose AA, Hueso R, Sánchez-Lavega A, Fisher RS, Rengstorf AW, Perelló C, Dascalu M, Altan M, Gazeas K, de Santana T, Sfair R, Winter OC, Kalkan S, Canales-Moreno O, Trigo-Rodríguez JM, Tsamis V, Tigani K, Sioulas N, Lekkas G, Bertesteanu DN, Dumitrescu V, Wilberger AJ, Barnes JW, Fieber-Beyer SK, Swaney RL, Fuentes C, Mendez RA, Dumitru BD, Flynn RL, Wake DA. 2023 A large topographic feature on the surface of the trans-Neptunian object (307261) 2002 MS₄ measured from stellar occultations. *A&A* **678**, A167. ([10.1051/0004-6361/202346892](https://doi.org/10.1051/0004-6361/202346892))
18. Rommel FL, Braga-Ribas F, Desmars J, Camargo JIB, Ortiz JL, Sicardy B, Vieira-Martins R, Assafin M, Santos-Sanz P, Duffard R, Fernández-Valenzuela E, Lecacheux J, Morgado BE, Benedetti-Rossi G, Gomes-Júnior AR, Pereira CL, Herald D, Hanna W, Bradshaw J, Morales N, Brimacombe J, Burtovoi A, Carruthers T, de Barros JR, Fiori M, Gilmore A, Hooper D, Hornoch K, Jacques C, Janik T, Kerr S, Kilmartin P, Winkel JM, Naletto G, Nardiello D, Nascimbeni V, Newman J, Ossola A, Pál A, Pimentel E, Pravec P, Sposetti S, Stechina A, Szakáts R, Ueno Y, Zampieri L, Broughton J, Dunham JB, Dunham DW, Gault D, Hayamizu T, Hosoi K, Jehin E, Jones R, Kitazaki K, Komžík R, Marciniak A, Maury A, Mikuž H, Nosworthy P, Fábrega Polleri J, Rahvar S, Sfair R, Siqueira PB, Snodgrass C, Sogorb P, Tomioka H, Tregloan-Reed J, Winter OC. 2020 Stellar occultations enable milliarcsecond astrometry for Trans-Neptunian objects and Centaurs. *A&A* **644**, A40. ([10.1051/0004-6361/202039054](https://doi.org/10.1051/0004-6361/202039054))
 19. Fraser WC, Bannister MT, Pike RE, Marsset M, Schwamb ME, Kavelaars JJ, Lacerda P, Nesvorný D, Volk K, Delsanti A, Benecchi S, Lehner MJ, Noll K, Gladman B, Petit JM, Gwyn S, Chen YT, Wang SY, Alexandersen M, Burdullis T, Sheppard S, Trujillo C. 2017 All planetesimals born near the Kuiper belt formed as binaries. *Nature Astronomy* **1**, 0088. ([10.1038/s41550-017-0088](https://doi.org/10.1038/s41550-017-0088))
 20. Nesvorný D, Vokrouhlický D. 2019 Binary survival in the outer solar system. *Icarus* **331**, 49–61. ([10.1016/j.icarus.2019.04.030](https://doi.org/10.1016/j.icarus.2019.04.030))
 21. Levison HF, Morbidelli A, Van Laerhoven C, Gomes R, Tsiganis K. 2008 Origin of the structure of the Kuiper belt during a dynamical instability in the orbits of Uranus and Neptune. *Icarus* **196**, 258–273. ([10.1016/j.icarus.2007.11.035](https://doi.org/10.1016/j.icarus.2007.11.035))
 22. Leinhardt ZM, Marcus RA, Stewart ST. 2010 The Formation of the Collisional Family Around the Dwarf Planet Haumea. *ApJ* **714**, 1789–1799. ([10.1088/0004-637X/714/2/1789](https://doi.org/10.1088/0004-637X/714/2/1789))
 23. Thirouin A, Sheppard SS. 2018 The Plutino Population: An Abundance of Contact Binaries. *AJ* **155**, 248. ([10.3847/1538-3881/aac0ff](https://doi.org/10.3847/1538-3881/aac0ff))
 24. Grundy WM, Noll KS, Roe HG, Buie MW, Porter SB, Parker AH, Nesvorný D, Levison HF, Benecchi SD, Stephens DC, Trujillo CA. 2019 Mutual orbit orientations of transneptunian binaries. *Icarus* **334**, 62–78. ([10.1016/j.icarus.2019.03.035](https://doi.org/10.1016/j.icarus.2019.03.035))
 25. Porter SB, Benecchi SD, Verbiscer AJ, Grundy WM, Noll KS, Parker AH. 2024 Detection of Close Kuiper Belt Binaries with HST WFC3. *Planetary Science Journal* **5**, 143. ([10.3847/PSJ/ad3f19](https://doi.org/10.3847/PSJ/ad3f19))
 26. Sicardy B, Bolt G, Broughton J, Dobosz T, Gault D, Kerr S, Bénard F, Frappa E, Lecacheux J, Peyrot A, Teng-Chuen-Yu JP, Beisker W, Boissel Y, Buckley D, Colas F, de Witt C, Doressoundiram A, Roques F, Widemann T, Gruhn C, Batista V, Biggs J, Dieters S, Greenhill J, Groom R, Herald D, Lade B, Mathers S, Assafin M, Camargo JIB, Vieira-Martins R, Andrei AH, da Silva Neto DN, Braga-Ribas F, Behrend R. 2011 Constraints on Charon's Orbital Elements from the Double Stellar Occultation of 2008 June 22. *AJ* **141**, 67. ([10.1088/0004-6256/141/2/67](https://doi.org/10.1088/0004-6256/141/2/67))
 27. Braga-Ribas F, Vachier F, Camargo J, Desmars J, Sicardy B, Vieira-Martins R, Assafin M, Benedetti-Rossi G, Dias-Oliveira A, Murakami Y, Lecacheux J. 2017 Stellar Occultations by TNOs: Probing Rings, Surface, and Satellites. In *Asteroids, Comets, Meteors (ACM2017)*, Montevideo, Uruguay.

28. Sickafoose AA, Bosh AS, Levine SE, Zuluaga CA, Genade A, Schindler K, Lister TA, Person MJ. 2019 A stellar occultation by Vanth, a satellite of (90482) Orcus. *Icarus* **319**, 657–668. ([10.1016/j.icarus.2018.10.016](https://doi.org/10.1016/j.icarus.2018.10.016))
29. Fernández-Valenzuela E, Ortiz Moreno JL, Holler B, Vara-Lubiano M, Morales N, Sicardy B, Vachier F, Desmars J, Braga-Ribas F, Jehin E, Rustamkulov Z, de la Vega A, Warner E, Benkhaldoun Z, Kamin R, Ryan A, Earls B, Conti D, de Wit J, Burdanov A, Richard F, Langill P, Morales R, Fraser W, Souami D, Lecacheux J, Santos-Sanz P, Duffard R, Alvarez-Candal A, Kretlow M, Benedetti-Rossi G, Morgado B, Camargo J, Rommel FL, Ramos Gomes Junior A, Assafin M, Baba Aissa D, Grigahcene Z, Buie M, Licandro J, Alarcon MR, Serra-Ricart M, Castro-Tirado A, Fernandez-Garcia EJ, Iglesias-Marzoa R, Galindo F, Pérez L, González H, Canedo P, Blanco O, Gonçalves R, Rengstorf A, Flynn R, Olsen A, Hanna B, Barnes J, A'Hearn JA, Kreyche SM, Miller WJ, Mortensen LE, Gibson TC, Walker G, McAllister GS, Feiden GA, Froetschel J, Steel S, Encardes D, Fisher RS, Luken A, Holcomb E, Caton D, Dunford B. 2021 Physical properties of Hi'iaka from stellar occultation data. In *AAS/Division for Planetary Sciences Meeting Abstracts* vol. 53AAS/Division for Planetary Sciences Meeting Abstracts p. 503.05.
30. Leiva R, Buie MW, Keller JM, Wasserman LH, Kavelaars J, Bridges T, Haley SL, Strauss R, Wilde E, Weryk R, Kervella P, Baker R, Bock SA, Conway K, Cota, Juan M. J, Estes JJ, García ML, Kehrl M, McCandless A, McCandless K, Self E, Settlemire C, Swanson DJ, Thompson D, Wise JA. 2020 Stellar Occultation by the Resonant Trans-Neptunian Object (523764) 2014 WC510 Reveals a Close Binary TNO. *Planetary Science Journal* **1**, 48. ([10.3847/PSJ/abb23d](https://doi.org/10.3847/PSJ/abb23d))
31. Fernandez-Valenzuela E, Holler B, Ortiz JL, Vachier F, Braga Ribas F, Rommel F, Desmars J, Buie M, Levine S, Collins M, Nikitin V, Skrutskie M, Collyer C, Pike R, Leiva R, Margoti G, Morales N, Verbiscer A, Stansberry J, DeColibus D, Castro Chacón J, Chanover N, McMillan R, Boyle R, Golden A, Butler R, Ryan M, Strauss R, Zigo H, Porter S, Kao M, Kretlow M, Vara-Lubiano M, Sicardy B, Pereira C, Santos-Sanz P, Morgado B, Benedetti-Rossi G. 2023 Weywot: the darkest known satellite in the trans-Neptunian region. In *AAS/Division for Planetary Sciences Meeting Abstracts* vol. 55AAS/Division for Planetary Sciences Meeting Abstracts p. 202.04.
32. Rommel FL, Fernández-Valenzuela E, Proudfoot BCN, Ortiz JL, Morgado BE, Sicardy B, Morales N, Braga-Ribas F, Desmars J, Vieira-Martins R, Holler BJ, Kilic Y, Grundy W, Rizos JL, Camargo JIB, Benedetti-Rossi G, Gomes-Júnior A, Assafin M, Santos-Sanz P, Kretlow M, Vara-Lubiano M, Leiva R, Ragozzine DA, Duffard R, Kučáková H, Hornoch K, Nikitin V, Santana-Ros T, Canales-Moreno O, Lafuente-Aznar D, Calavia-Belloc S, Perelló C, Selva A, Organero F, Hernandez LA, de la Cueva I, Yuste-Moreno M, García-Navarro E, Donate-Lucas JE, Izquierdo-Carrión L, Iglesias-Marzoa R, Lacruz E, Gonçalves R, Staels B, Goossens R, Henden A, Walker G, Reyes JA, Pastor S, Kaspi S, Skrutskie M, Verbiscer AJ, Martinez P, André P, Maestre JL, Aceituno FJ, Bacci P, Maestripieri M, Grazia MD, Castro-Tirado AJ, Pérez-García I, Fernández García EJ, Fernández E, Messner S, Scarfi G, Mikuž H, Prat J, Martorell P, Nardiello D, Nascimbeni V, Sfair R, Siqueira PB, Lattari V, Liberato L, Pinheiro TFL, de Santana T, Pereira CL, Alava-Amat MA, Ciabattari F, González-Rodríguez H, Schnabel C. 2025 Stellar occultation observations of (38628) Huya and its satellite: a detailed look into the system. *arXiv e-prints* p. arXiv:2501.09739.
33. Vara-Lubiano M, Fernández-Valenzuela E, Kretlow M, Morales N, Benedetti-Rossi G, Rommel F, Ortiz JL, Sicardy B, Santos-Sanz P, Vieira-Martins R, Braga-Ribas F, Camargo J, Kilic Y, Morgado B, Gomes A, Alvarez-Candal A, Lecacheux J, Assafin M, Duffard R, Souami D, Desmars J, Mottola S, Sota A, Pal A, Szakáts R, Kiss C, Kalup C, Derekas A, Zejmo M, Marciniak A, Ogloza W, Dangl G, Carbognani A, Stirpe G, Bruni I, Csányi I, Skvarč J, Mikuz H, Meister S, Conjat M, Ciabattari F, Krannich G. 2023 Updated Size of the Trans-Neptunian Binary 2000 YW134 from a Stellar Occultation. In *Planetary Sciences and Exploration of the Solar System (7th CPESS)* p. 80575.
34. Leiva R, Ortiz JL, Gómez-Limón JM, Perez P, Kretlow M, Desmars J, Morales N, Rommel FL, Margoti G, Vara-Luviano M, Santos-Sanz P, Duffard R, Rizos JL, Fernandez-Valenzuela E, Braga-Ribas F, Liberato Mendes L, Malacarne M, Gomes-Jr AR, Sfair R. 2023 (470316) 2007 OC10, (470309) 2007 JK43, and (19521) Chaos, Results from Stellar Occultations. In *LPI Contributions* vol. 2851LPI Contributions p. 2527.
35. Braga-Ribas F, Crispim A, Vieira-Martins R, Sicardy B, Ortiz JL, Assafin M, Camargo JIB, Desmars J, Lecacheux J, Santos-Sanz P, Duffard R, Benedetti-Rossi G, Gomes-Júnior AR,

- Morgado B, Rommel FL, Margoti G, Pereira CL. 2019 Database on detected stellar occultations by small outer Solar System objects. In *Journal of Physics Conference Series* vol. 1365 *Journal of Physics Conference Series* p. 012024. ([10.1088/1742-6596/1365/1/012024](https://doi.org/10.1088/1742-6596/1365/1/012024))
36. Araujo RAN, Sfair R, Winter OC. 2016 The Rings of Chariklo under Close Encounters with the Giant Planets. *ApJ* **824**, 80. ([10.3847/0004-637X/824/2/80](https://doi.org/10.3847/0004-637X/824/2/80))
 37. Sicardy B, Renner S, Leiva R, Roques F, El Moutamid M, Santos-Sanz P, Desmars J. 2020 Chapter 11 - The dynamics of rings around Centaurs and Trans-Neptunian objects. In Prialnik D, Barucci MA, Young LA, editors, *The Trans-Neptunian Solar System*, pp. 249–269. Elsevier. (<https://doi.org/10.1016/B978-0-12-816490-7.00011-4>)
 38. Gaia Collaboration et al.. 2023 Gaia Data Release 3. Summary of the content and survey properties. *A&A* **674**, A1. ([10.1051/0004-6361/202243940](https://doi.org/10.1051/0004-6361/202243940))
 39. Vachier F, Berthier J, Marchis F. 2012 Determination of binary asteroid orbits with a genetic-based algorithm. *A&A* **543**, A68. ([10.1051/0004-6361/201118408](https://doi.org/10.1051/0004-6361/201118408))
 40. Vachier F, Carry B, Berthier J. 2022 Dynamics of the binary asteroid (379) Huenna. *Icarus* **382**, 115013. ([10.1016/j.icarus.2022.115013](https://doi.org/10.1016/j.icarus.2022.115013))
 41. Yang B, Wahhaj Z, Beauvalet L, Marchis F, Dumas C, Marsset M, Nielsen EL, Vachier F. 2016 Extreme AO Observations of Two Triple Asteroid Systems with SPHERE. *ApJ* **820**, L35. ([10.3847/2041-8205/820/2/L35](https://doi.org/10.3847/2041-8205/820/2/L35))
 42. Proudfoot BCN, Ragozzine DA, Thatcher ML, Grundy W, Spencer DJ, Alailima TM, Allen S, Bowden PC, Byrd S, Camacho CD, Campbell GH, Carlisle EP, Christensen JA, Christensen NK, Clement K, Derieg BJ, Dille MK, Dorrett C, Ellefson AL, Fleming TS, Freeman NJ, Gibson EJ, Giforos WG, Guerrette JA, Haddock O, Hammond SA, Hampson ZA, Hancock JD, Harmer MS, Henderson JR, Jensen CR, Jensen D, Jensen RE, Jones JS, Kubal CC, Lunt JN, Martins S, Matheson M, Maxwell D, Morrell TD, Myckowiak MM, Nelsen MA, Neu ST, Nuccitelli GG, Reardon KM, Reid AS, Richards KG, Robertson MRW, Rydalch TD, Scoresby CB, Scott RL, Shakespear ZD, Silveira EA, Steed GC, Suggs CZ, Suggs GD, Tobias DM, Toole ML, Townsend ML, Vickers KL, Wagner CR, Wright MS, Zappala EMA. 2024 Beyond Point Masses. II. Non-Keplerian Shape Effects Are Detectable in Several TNO Binaries. *AJ* **167**, 144. ([10.3847/1538-3881/ad26f0](https://doi.org/10.3847/1538-3881/ad26f0))
 43. Desmars J et al.. 2015 Orbit determination of trans-Neptunian objects and Centaurs for the prediction of stellar occultations. *A&A* **584**, A96. ([10.1051/0004-6361/201526498](https://doi.org/10.1051/0004-6361/201526498))
 44. Ferreira JF, Tanga P, Machado P, Corsaro E. 2020 A survey for occultation astrometry of main belt: expected astrometric performances. *A&A* **641**, A81. ([10.1051/0004-6361/202038190](https://doi.org/10.1051/0004-6361/202038190))
 45. Camargo JIB, Desmars J, Braga-Ribas F, Vieira-Martins R, Assafin M, Sicardy B, Bérard D, Benedetti-Rossi G. 2018 The future of stellar occultations by distant solar system bodies: Perspectives from the Gaia astrometry and the deep sky surveys. *Planet. Space Sci.* **154**, 59–62. ([10.1016/j.pss.2018.02.014](https://doi.org/10.1016/j.pss.2018.02.014))
 46. Benedetti-Rossi G, Vieira Martins R, Camargo JIB, Assafin M, Braga-Ribas F. 2014 Pluto: improved astrometry from 19 years of observations. *A&A* **570**, A86. ([10.1051/0004-6361/201424275](https://doi.org/10.1051/0004-6361/201424275))
 47. Berdeu A, Langlois M, Vachier F. 2022 First observation of a quadruple asteroid. Detection of a third moon around (130) Elektra with SPHERE/IFS. *A&A* **658**, L4. ([10.1051/0004-6361/202142623](https://doi.org/10.1051/0004-6361/202142623))
 48. Brown ME, Butler BJ. 2023 Masses and Densities of Dwarf Planet Satellites Measured with ALMA. *Planetary Science Journal* **4**, 193. ([10.3847/PSJ/ace52a](https://doi.org/10.3847/PSJ/ace52a))
 49. Brown ME, Ragozzine D, Stansberry J, Fraser WC. 2010 The Size, Density, and Formation of the Orcus-Vanth System in the Kuiper Belt. *AJ* **139**, 2700–2705. ([10.1088/0004-6256/139/6/2700](https://doi.org/10.1088/0004-6256/139/6/2700))
 50. Carry B, Hestroffer D, DeMeo FE, Thirouin A, Berthier J, Lacerda P, Sicardy B, Doressoundiram A, Dumas C, Farrelly D, Müller TG. 2011 Integral-field spectroscopy of (90482) Orcus-Vanth. *A&A* **534**, A115. ([10.1051/0004-6361/201117486](https://doi.org/10.1051/0004-6361/201117486))
 51. Camargo JIB, Vieira-Martins R, Assafin M, Braga-Ribas F, Sicardy B, Desmars J, Andrei AH, Benedetti-Rossi G, Dias-Oliveira A. 2014 Candidate stellar occultations by Centaurs and trans-Neptunian objects up to 2014. *A&A* **561**, A37. ([10.1051/0004-6361/201322579](https://doi.org/10.1051/0004-6361/201322579))

52. Brown ME, Butler BJ. 2018 Medium-sized Satellites of Large Kuiper Belt Objects. *AJ* **156**, 164. ([10.3847/1538-3881/aad9f2](https://doi.org/10.3847/1538-3881/aad9f2))
53. Ortiz JL, Gutiérrez PJ, Sota A, Casanova V, Teixeira VR. 2003 Rotational brightness variations in Trans-Neptunian Object 50000 Quaoar. *A&A* **409**, L13–L16. ([10.1051/0004-6361:20031253](https://doi.org/10.1051/0004-6361:20031253))
54. Brown ME, Suer TA. 2007 Satellites of 2003 AZ₈₄, (50000), (55637), and (90482). *IAU Circ.* **8812**, 1.
55. Fornasier S, Lellouch E, Müller T, Santos-Sanz P, Panuzzo P, Kiss C, Lim T, Mommert M, Bockelée-Morvan D, Vilenius E, Stansberry J, Tozzi GP, Mottola S, Delsanti A, Crovisier J, Duffard R, Henry F, Lacerda P, Barucci A, Gicquel A. 2013 TNOs are Cool: A survey of the trans-Neptunian region. VIII. Combined Herschel PACS and SPIRE observations of nine bright targets at 70–500 μm . *A&A* **555**, A15. ([10.1051/0004-6361/201321329](https://doi.org/10.1051/0004-6361/201321329))
56. Fraser WC, Batygin K, Brown ME, Bouchez A. 2013 The mass, orbit, and tidal evolution of the Quaoar-Weywot system. *Icarus* **222**, 357–363. ([10.1016/j.icarus.2012.11.004](https://doi.org/10.1016/j.icarus.2012.11.004))
57. Elliot JL, Dunham EW, Bosh AS, Slivan SM, Young LA, Wasserman LH, Millis RL. 1989 Pluto's atmosphere. *Icarus* **77**, 148–170. ([10.1016/0019-1035\(89\)90014-6](https://doi.org/10.1016/0019-1035(89)90014-6))
58. Brosch N. 1995 The 1985 stellar occultation by Pluto. *MNRAS* **276**, 571–578. ([10.1093/mnras/276.2.571](https://doi.org/10.1093/mnras/276.2.571))
59. Elliot JL, Person MJ, Zuluaga CA, Bosh AS, Adams ER, Brothers TC, Gulbis AAS, Levine SE, Lockhart M, Zangari AM, Babcock BA, Dupré K, Pasachoff JM, Souza SP, Rosing W, Secrest N, Bright L, Dunham EW, Sheppard SS, Kakkala M, Tilleman T, Berger B, Briggs JW, Jacobson G, Vallemi P, Volz B, Rapoport S, Hart R, Brucker M, Michel R, Mattingly A, Zambrano-Marin L, Meyer AW, Wolf J, Ryan EV, Ryan WH, Morzinski K, Grigsby B, Brimacombe J, Ragozzine D, Montano HG, Gilmore A. 2010 Size and albedo of Kuiper belt object 55636 from a stellar occultation. *Nature* **465**, 897–900. ([10.1038/nature09109](https://doi.org/10.1038/nature09109))
60. Marques Oliveira J, Sicardy B, Gomes-Júnior AR, Ortiz JL, Strobel DF, Bertrand T, Forget F, Lellouch E, Desmars J, Bérard D, Doressoundiram A, Lecacheux J, Leiva R, Meza E, Roques F, Souami D, Widemann T, Santos-Sanz P, Morales N, Duffard R, Fernández-Valenzuela E, Castro-Tirado AJ, Braga-Ribas F, Morgado BE, Assafin M, Camargo JIB, Vieira-Martins R, Benedetti-Rossi G, Santos-Filho S, Banda-Huarca MV, Quispe-Huaynasi F, Pereira CL, Rommel FL, Margoti G, Dias-Oliveira A, Colas F, Berthier J, Renner S, Hueso R, Pérez-Hoyos S, Sánchez-Lavega A, Rojas JF, Beisker W, Kretlow M, Herald D, Gault D, Bath KL, Bode HJ, Bredner E, Guhl K, Haymes TV, Hummel E, Kattentidt B, Klös O, Pratt A, Thome B, Avdellidou C, Gazeas K, Karampotsiou E, Tzouganas L, Kardasis E, Christou AA, Xilouris EM, Alikakos I, Gourzelas A, Liakos A, Charmandaris V, Jelínek M, Štrobl J, Eberle A, Rapp K, Gährken B, Klemt B, Kowollik S, Bitzer R, Miller M, Herzogenrath G, Frangenberg D, Brandis L, Pütz I, Perdelwitz V, Piehler GM, Riepe P, von Poschinger K, Baruffetti P, Cenadelli D, Christille JM, Ciabattari F, Di Luca R, Alboresi D, Leto G, Zanmar Sanchez R, Bruno P, Occhipinti G, Morrone L, Cupolino L, Noschese A, Vecchione A, Scalia C, Lo Savio R, Gardina G, Kamoun S, Barbosa R, Behrend R, Spano M, Bouchet E, Cottier M, Falco L, Gallego S, Tortorelli L, Sposetti S, Sussenbach J, Van Den Abbeel F, André P, Llibre M, Paillet F, Ardissonne J, Boutet M, Sanchez J, Bretton M, Cailleau A, Pic V, Granier L, Chauvet R, Conjat M, Dauvergne JL, Dechambre O, Delay P, Delcroix M, Rousselot L, Ferreira J, Machado P, Tanga P, Rivet JP, Frappa E, Irzyk M, Jabet F, Kaschinski M, Klotz A, Rieugnie Y, Klotz AN, Labrevois O, Lavandier D, Walliang D, Leroy A, Bouley S, Lisciandra S, Coliac JF, Metz F, Erpelding D, Nougayrède P, Midavaine T, Miniou M, Moindrot S, Morel P, Reginato B, Reginato E, Rudelle J, Tregon B, Tanguy R, David J, Thuillot W, Hestroffer D, Vaudescal G, Baba Aissa D, Grigahcene Z, Briggs D, Broadbent S, Denyer P, Haigh NJ, Quinn N, Thurston G, Fossey SJ, Arena C, Jennings M, Talbot J, Alonso S, Román Reche A, Casanova V, Briggs E, Iglesias-Marzoa R, Abril Ibáñez J, Díaz Martín MC, González H, Maestre García JL, Marchant J, Ordonez-Etxeberria I, Martorell P, Salamero J, Organero F, Ana L, Fonseca F, Peris V, Brevia O, Selva A, Perello C, Cabedo V, Gonçalves R, Ferreira M, Marques Dias F, Daassou A, Barkaoui K, Benkhaldoun Z, Guennoun M, Chouqar J, Jehin E, Rinner C, Lloyd J, El Moutamid M, Lamarche C, Pollock JT, Caton DB, Kouprianov V, Timerson BW, Blanchard G, Payet B, Peyrot A, Teng-Chuen-Yu JP, Françoise J, Mondon B, Payet T, Boissel C, Castets M, Hubbard WB, Hill R, Reitsemá HJ, Mousis O, Ball L, Neilsen G, Hutcheon S, Lay K, Anderson P, Moy M, Jonsen M, Pink I, Walters R, Downs B. 2022 Constraints on the structure and seasonal variations of

Triton's atmosphere from the 5 October 2017 stellar occultation and previous observations. *A&A* **659**, A136. ([10.1051/0004-6361/202141443](https://doi.org/10.1051/0004-6361/202141443))

61. Sallum S, Millar-Blanchaer MA, Batalha N, Wang J, Martinez R, Fitzgerald MP, Skemer A, Jensen-Clem R, Mazin BA, Chun M, Guyon O, Hinz P, Males J, Max C. 2022 The Planetary Systems Imager for TMT: driving science cases and top level requirements. In Evans CJ, Bryant JJ, Motohara K, editors, *Ground-based and Airborne Instrumentation for Astronomy IX* vol. 12184 *Society of Photo-Optical Instrumentation Engineers (SPIE) Conference Series* p. 1218446. International Society for Optics and Photonics SPIE. ([10.1117/12.2630423](https://doi.org/10.1117/12.2630423))

62. Sicardy B, Leiva R, Renner S, Roques F, El Moutamid M, Santos-Sanz P, Desmars J. 2019 Ring dynamics around non-axisymmetric bodies with application to Chariklo and Haumea. *Nature Astronomy* **3**, 146–153. ([10.1038/s41550-018-0616-8](https://doi.org/10.1038/s41550-018-0616-8))